MIXED-MODE INTERFACIAL FRACTURE TOUGHNESS OF SANDWICH COMPOSITES AT CRYOGENIC TEMPERATURES

By

WON-JONG NOH

A THESIS PRESENTED TO THE GRADUATE SCHOOL
OF THE UNIVERSITY OF FLORIDA IN PARTIAL FULFILLMENT OF THE
REQUIREMENTS FOR THE DEGREE OF MASTER OF SCIENCE

UNIVERSITY OF FLORIDA

2004

This document is dedicated to the graduate students of the University of Florida.

ACKNOWLEDGMENTS

It is appropriate at this point to acknowledge the people that have made this research possible. Without the support and guidance of Dr. B.V. Sankar, this research would not have been possible. He has been my adviser and sponsor during my entire academic and research experience at the University of Florida. He is a generous and intelligent person who can lead and advise many people academically. Also I want to say thanks to Dr. C.C. Hsu for his advice and help at the beginning of my graduate school.

Doing my research work, I received a lot of help and advice from my colleagues at the Center for Advanced Composites. They are very friendly and open-minded people, so I had a good relationship with them. In addition to academic work, they have also made me have a lot of fun and unforgettable memories in the U.S. So I would like to thank all of them, too.

Like other research, without funding it would not have been possible to do this research. The people at NASA Glenn Research Center supported this project from the beginning to the end. Glenn Research Center supported the grant (NAG3-2750) and cooperated with the Center for Advanced Composites and the University of Florida.

Finally I appreciate my parents, Soo-Kyoung Noh and Keum-Sik Min, and my sisters, Sun-Ju and Sun-Hee. They give me valuable mental and material support during my school life and U.S. life.

TABLE OF CONTENTS

page

LIST OF TABLES

LIST OF FIGURES

Abstract of Thesis Presented to the Graduate School
of the University of Florida in Partial Fulfillment of the
Requirements for the Degree of Master of Science

MIXED-MODE INTERFACIAL FRACTURE TOUGHNESS OF SANDWICH COMPOSITES AT CRYOGENIC TEMPERATURES

By

Won-Jong Noh

August 2004

Chair: Bhavani V. Sankar
Major Department: Mechanical and Aerospace Engineering

The aim of this study is to understand the failure phenomena of sandwich composites constructed from carbon fiber/epoxy composite face-sheets and Nomex honeycomb core under cryogenic conditions. Both experimental testing and finite element analysis are performed to understand the conditions under which face sheet debonding occurs and propagates. One of the major objectives of this study is to measure the critical energy release rate or fracture toughness of the face sheet/core interface, which will be a strong function of mode-mixity and temperature. Furthermore, mode-mixity itself will depend on geometric factors such as crack length, face sheet and core thickness and material stiffness parameters.

Fracture tests similar to double cantilever beam tests are performed on sandwich panels containing initial delaminations. The fracture toughness is measured for various crack lengths. The loads at which crack propagation occurs are applied in the finite element model of the panel to obtain the detailed stress field in the vicinity of the crack

tip. From the results of the fracture tests and finite element analyses, it is found that the interfacial fracture toughness of the sandwich composites decreases significantly at cryogenic temperatures.

CHAPTER 1
INTRODUCTION

Background Information

Honeycomb sandwich composites are found in a wide range of structural applications due to their high strength and stiffness-to-weight ratio compared to other systems. Current use of sandwich composites ranges from secondary structures in commercial aircrafts to primary structures in military aircrafts, helicopters, and reusable launch vehicles (RLV), e.g., Space Shuttle. One of applications of sandwich construction is the liquid hydrogen tank of future RLV. Because of its low density and high stiffness, sandwich construction is attractive for LH_2 tanks. However, past tests have shown that leakage of hydrogen through the composite face-sheets and subsequent debonding of the face-sheets is one of the major concerns in using sandwich construction. This problem can be eliminated by thorough understanding of the fracture mechanics of face sheets under cryogenic conditions.

Delamination is a particularly serious damage mode for high-performance laminated sandwich composites. The double cantilever test (DCB) has been used frequently to characterize the delamination resistance of laminates, and the energy area method has been used to perform experimental analyses. Finite element analyses (FE) are performed complementarily to investigate the stress intensity factor (SIF), the energy release rate (G) and the phase angle (Ψ) for mode-mixity in the vicinity of the crack-tip area.

The fracture mechanics analysis of a delamination between the core and the face sheet is complicated by the fact that the crack-tip stress fields have the complex oscillatory characteristics and bi-material fracture mechanics concepts have to be used. Ducept et al.[1] performed global, local and numerical methods to describe the failure phenomena around the crack-tip and found that the local and numerical method values were close to each other, while global method values were quite different.

Literature Review

Research has been conducted to predict the thermal effect on the stress intensity factor, the energy release rate and the mode mixity at room temperature and also at cryogenic temperature using several approaches. Grau [2] modeled sandwich composites with pre-crack at the core/face-sheet interface at the edge of panels. Sandwich panels with honeycomb cores were modeled as a double cantilever beam (DCB) wherein orthotropic properties were used for the core of the commercial FE software ABAQUS was used to build 2D and 3D models for various crack lengths of the sandwich composites.

Cryogenic chamber and testing methods, created by Johnson, Melcher, and Pavlick in the Mechanical Properties Research Lab at Georgia Institute of Technology, were used to investigate tensile properties and fracture toughness.

Schutz [3] has provided a compilation of test data for several material systems. In general, he showed that static properties such as tensile modulus, tensile strength and compressive strength all increased as the test temperature was decreased from 300 K to 77 K. It was also found that thermal stresses had a large influence on failure behavior and that the temperature dependent properties of the material system could be used to help to explain the stress-strain response of laminated composites. For compression loading,

Gates et al.[4] discovered that cryogenic temperatures produced an increase in both the modulus and the strength of all the laminates. The greatest increase in compressive strength occurred in the laminates with a 90-degree orientation. The greatest increase in modulus occurred in the laminates with a 45-degree orientation.

Bitzer [5] explained that normally provided honeycomb properties are the compressive strength modulus in the T direction and the shear strengths and moduli in the LT and WT directions. The properties not provided by company are seldom tested as they are extremely minimal. In some finite element programs, the Poisson's ratio of the material must be entered or the program will not run. Usually the honeycomb core moduli are so much smaller than the facings that it does not matter what honeycomb Poisson's ratio value is assumed. He advised to use a honeycomb Poisson's ratio of 0.1 in the FE program, then use 0.5 and see if there was any difference in the results. This procedure would show the program sensitivity to the honeycomb Poisson's ratio.

The fracture toughness of the bond line was measured through the double cantilever beam test by Ural et al.[6] at room and low temperatures. In order to investigate the effect of mode-mixity on G_c values, they performed numerical simulations. Those analyses showed that not only the mode-mixity was low, but also it did not change significantly with crack length. For each crack growth step, the corresponding energy release rate was calculated and these values were averaged to obtain a single G_c value. The experiment was complementary to the numerical work. Thus tensile strength and fracture toughness of the face-sheets/core bond, measured by the experiments, were used as parameters for simulation of the delamination and propagation tests. As expected, low temperature tests resulted in decreased values of G_c.

This shows that a decrease in temperature leads to a more critical state for the material and the error involved in the calculation of G_c depends on the measurement of the load, P, and the crack length, a. They referred that possible error included in the measurement of P is 0.5% of the load range.

Suo [7] derived the necessary equations and developed the fracture mechanics concepts necessary for interfacial fracture mechanics of anisotropic solids. For bonded orthotropic materials, a complex-variable representation is presented for a class of degenerated orthotropic materials. The work came from both historical and recent experiments and theoretical investigations of several research groups on fracture behaviors of woods, composites, bicrystals and oriented polymers. To gain more insight, Suo derived the necessary equations relating to orthotropic materials. This is shown in Appendix A.

Scope of the Thesis

The next-generation RLV will have an internal liquid-hydrogen fuel tank that not only functions as a container for the fuel but must also perform as a load-carrying structure during launch and flight operations. Presently, it appears that the replacement of traditional metallic cryogenic fuel tanks with composite tanks may lead to significant weight reduction and hence increased load-carrying capabilities.

The scope of the present research is to assess the thermal/mechanical phenomena of sandwich composites at cryogenic temperatures, document the test methods, and provide insight into the effects of temperature on mechanical performance. The selected test methods include a range of crack lengths, core thicknesses, loads and temperatures which could be experienced during the usage of cryogenic hydrogen tanks. It is expected that

the results of this study will be important in the development of future material qualification methods and design verification.

CHAPTER 2
SPECIMEN AND TEST SETUP

Experimental Setup

Specimen Preparation

Sandwich specimens used in this study consist of Toray Composites unidirectional carbon fiber prepreg as face-sheets and Euro Composites aramid fiber ECA type honeycomb as the core material. Sandwich panels of size 10 in. × 10 in. were constructed and specimens were machined from the panel for various tests. In order to obtain and test specimens from the sandwich panels, several tasks have to be completed in the following order: fabricating sandwich composites; machining out beams; attaching tabs to the beams; and painting the interface region for the purpose of crack detection.

Typically, an adhesive layer is placed between the core and face-sheets during a co-curing cycle to promote better adhesion. However, due to the properties of the prepreg material (typically prepreg contains 40 % resin/adhesive) it is decided that a direct lay-up of the prepreg onto the top of the honeycomb core will provide sufficient bonding strength. This method has also been verified by Grau [2].

The next sequence includes laying the unidirectional fiber tapes within the face-sheets. Several previous tests were performed to find the optimum specimen. It is necessary to note that the lay-up should be symmetric when layering the unidirectional prepreg. If the layering for face-sheets is not symmetric, residual stresses that will likely result in warping of the sandwich panel will develop after curing [8]. Teflon sheet

(PTFE) laid between the core and the face sheet will produce a delamination, as shown in Figure 2.1.

Vacuum bagging is used as the system for applying vacuum to the sandwich lay-up during the cure cycle. The lay-up sequence is as follows: A 0.5 in. sheet of aluminum is used as a base tool; a Non-porous Teflon film (PTFE) is placed above the tool to release the sandwich after the cure cycle; an 8 ply $[0/90]_{2S}$ face sheet is laid as the bottom side of the sandwich; then a Nomex honeycomb core with a designated thickness of either 1 in., 0.5 in. or 0.25 in. is placed on top of the bottom face-sheets; a strip of PTFE is used to create the artificial crack between the core and the top face-sheets; then another 8 ply face-sheet is used on top of the core/PTFE strip; a PTFE sheet is placed over top of the sandwich; finally, a breather material is laid on top of the other components to allow for adequate air evacuation during the vacuum process. A vacuum port is installed in the bag material near the edge of the tool to ensure it does not affect the sandwich. Figure 2.1 shows the schematic lay-up design without the vacuum port. Figure 2.2, shows an actual lay-up before and after the vacuum bag is sealed. All of the material and its suppliers are documented in Appendix D. It is necessary to note that the release film used is not porous and therefore will not allow any excess epoxy to flow from the prepreg to the breather. This lay-up design requires all of the epoxy to remain in the sandwich to ensure adequate bonding strength.

However, when this method is used to create the sandwich panels described in Appendix D the pressure crushes the cores in the in-plane directions (L or W direction). After further testing, the Toray cure cycle was modified with no pressure and with a nominal vacuum of 23 psig. Using only a vacuum, a sandwich composite with sufficient

adhesion between the face-sheets and the core was created. It should be noted that further experimentation was conducted to evaluate the newly tested material properties. However, for all of the experimentation documented in this thesis, the cure cycle is used with no autoclave pressure. Figure 2.3 shows the autoclave with a lay-up inserted before the cure cycle has begun.

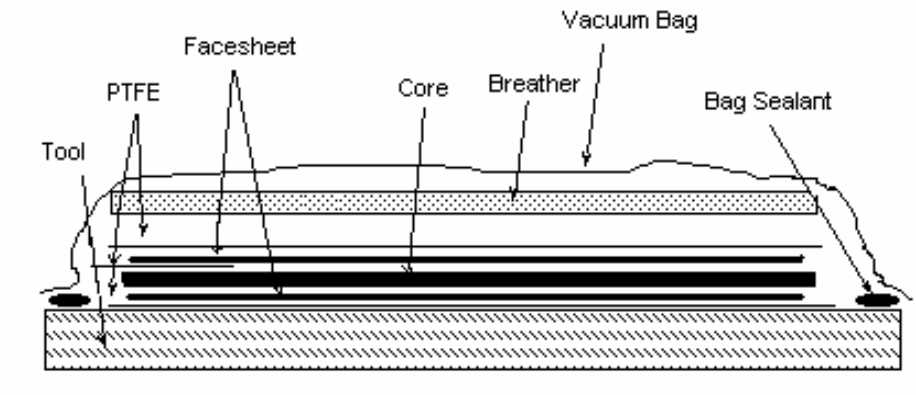

Figure 2.1 Preparation of vacuum bag.

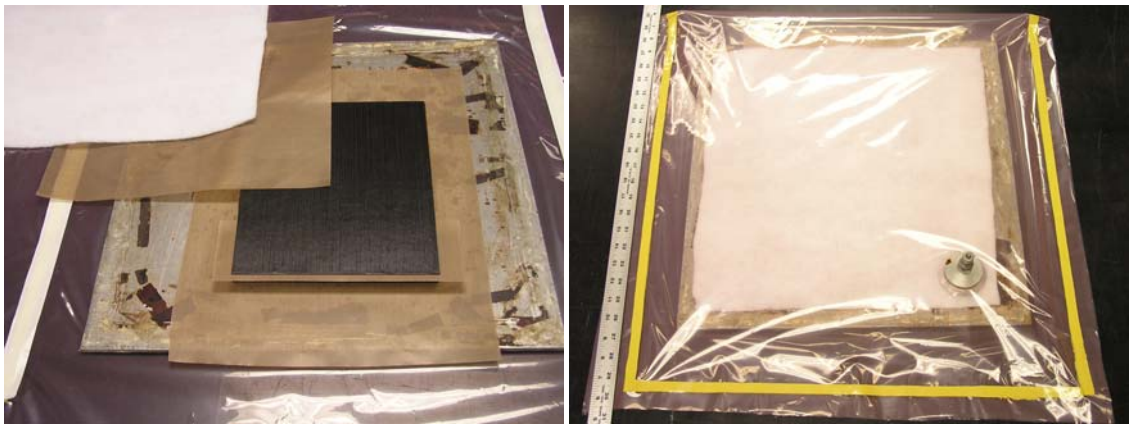

Figure 2.2 Preparation of vacuum bag before and after the vacuum bag is sealed.

Eight specimens were machined from each of the sandwich panels. The specimens were cut from the panels using a water-cooled tile saw with a diamond-coated blade. Honeycomb core sandwich materials are difficult to machine because of the heat and debris generated by traditional machining. Slow cutting with the water-cooled tile saw negated those problems. While parallel cutting can be made, the width varies from

specimen to specimen. Even though the width varies on each specimen, the overall width did not vary in relation to the overall length. The average width of all specimens is regarded as one inch.

Figure 2.3 Autoclave before a cure cycle runs.

After machining the specimen to its final dimensions (6.5 in. × 1.0 in.), aluminum piano hinges are adhesively bonded to both sides of the sandwich composites as shown in Figure 2.4. Piano hinges function as load introduction points for the specimen. One side of the hinge is connected with a load-cell. Another part of the hinge is gripped by testing machines.

Figure 2.4 Specimen preparation: (a) Specimen bonding with loading taps, (b) The painted interface.

White paint (typing correction fluid) has been applied to the interfacial surface of the specimen over the region where the crack is expected to grow. Using a fine tip pen, points have been made at 1.0 inch along the interface region.

Cryogenic Environmental Chamber

For several types of in-situ cryogenic tests, four-point bending tests, and fracture toughness tests, a facility for exposing the specimens to LN_2 had not previously existed at the Center for Advanced Composites (CAC) of University of Florida. The CAC has only a cryogenic chamber, EC-12, which is not suitable for in-situ cryogenic tests. With the courtesy of Dr. W.S. Johnson in MPRL at the Georgia Institute of Technology, and Dr. Ihas, Professor of Physics at the University of Florida, a cryogenic environmental chamber, consisting of a double-walled structure, was fabricated. The chamber consists of two different-sized buckets and the expanding foam of DOW which functions as an insulation material between the two buckets. The base has a hole to allow a pull-rod to pass through for both 4-point bending and fracture toughness tests. A silicon-stopper was installed into a hole to prevent LN_2 from leaking out from it. Upon testing with LN_2 and consulting with the lab technician in the UF Physics department's Cryogenic Lab, plastic bags were used as an additional sealing precaution, because of their high tear resistance and high puncture resistance. The perfectly insulated LN_2 storage in the CAC is not equipped for recycling, therefore the used LN_2 should be vaporized after every test has been completed. The cryogenic chamber at the CAC is shown in Figures 2.5 and 2.6.

Figure 2.6 depicts the entire test setup for in-situ cryogenic test environment. The liquid nitrogen tank has a steel hose to dispense it into chamber. For safety purposes personal equipment, such as leather gloves, face shields, and aprons, should be used carefully once the in-situ cryogenic tests are being performed.

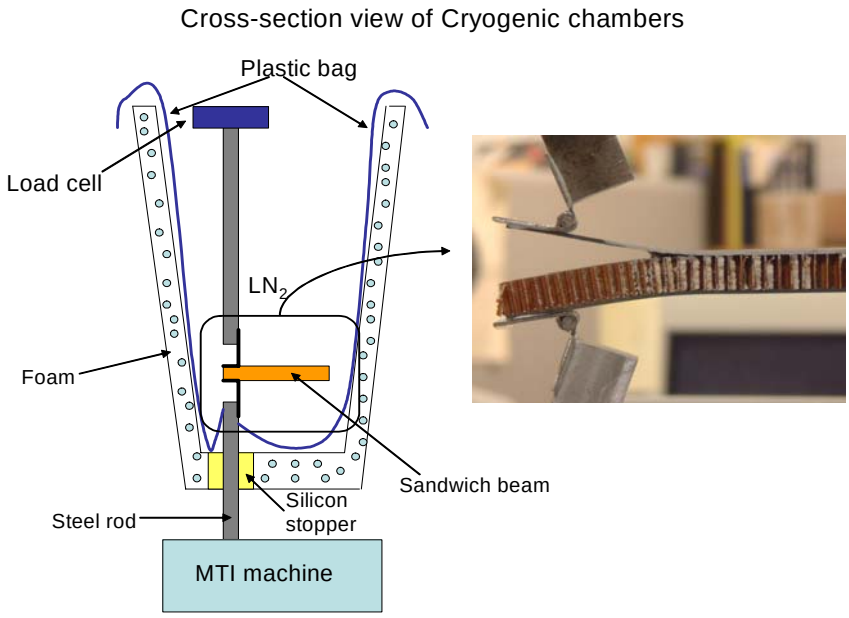

Figure 2.5 Cross section view of cryogenic chamber.

Figure 2.6 Entire cryogenic test setup during dispensing of LN_2.

Experimental Procedure

In order to calculate the fracture toughness of the interface, an accurate experimental technique must be used. Various experimental configurations have been reviewed that include tests for a double cantilever beam (DCB) and for four point bending. After some consideration, the DCB test was chosen for determining the interfacial fracture toughness of the sandwich composite, due to the ease of the test and its relative high accuracy. Experimental procedures presented in this thesis utilize a double cantilever beam comprised of layered carbon fiber composite face sheets bonded to a Nomex® honeycomb core.

In principle the DCB test is quite simple. A specimen is prepared with an initial crack of length *a* within the interface, where the fracture toughness is of interest. The specimen is then placed in a loading test fixture created specifically for the DCB test. Loading of the specimen occurs such that the surfaces lying on the interface are separated as shown in Figure 2.7.

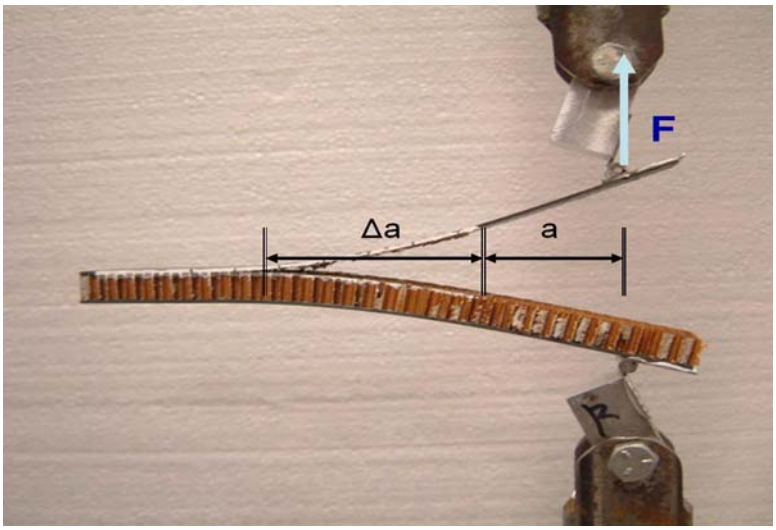

Figure 2.7 Double cantilever beam test (DCB) loading.

The fracture tests were carried out in a 12,000-lb. MTI test machine using a 5000-lb. load-cell. Two piano hinges are attached to the pull-rod of the crosshead. All tests

were conducted in displacement control with a crosshead loading rate of 0.05 in./min. Force and displacement were recorded using a data-acquisition card installed in the computer throughout the loading and unloading of each test. By an optical microscope (see Figure 2.8), the whole sequence and the phenomena of crack propagation was observed and controlled manually.

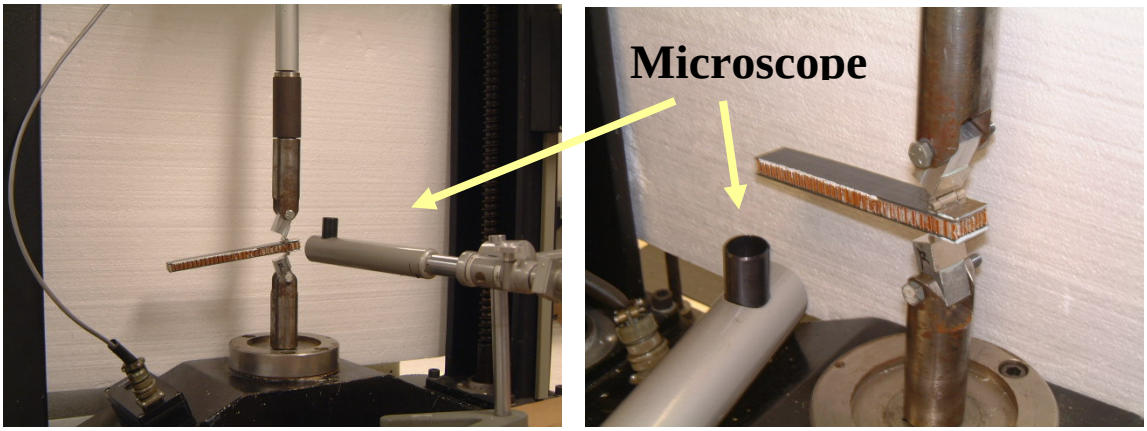

Figure 2.8 Observation specimens with a microscope.

First, the initial crack was recorded at the beginning of testing. The movement of the MTI crosshead was controlled and monitored along the crack propagation. The specimen was loaded with a specific loading rate until the crack reached the 1.0 inch mark or the force dropped suddenly, as shown in Figure 2.9.

Once the new crack-tip length was checked and recorded, the direction of the crosshead was reversed and the related data was recorded. Next, to investigate the effect of cryogenic temperatures on the fracture toughness of sandwich composites, the DCB test was performed in liquid nitrogen at 77K. Because the specimen is submerged in a plastic insulated vessel at an extremely low temperature (as shown in Figure 2.10) it is impossible to monitor crack propagation.

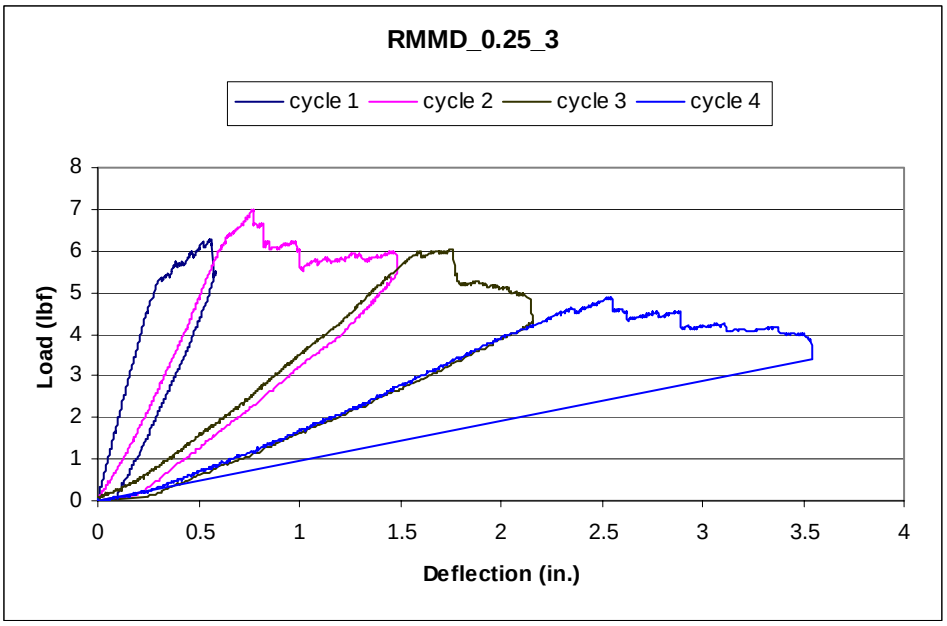

Figure 2.9 Typical example of loading graph during mixed-mode DCB test at cryogenic temperature.

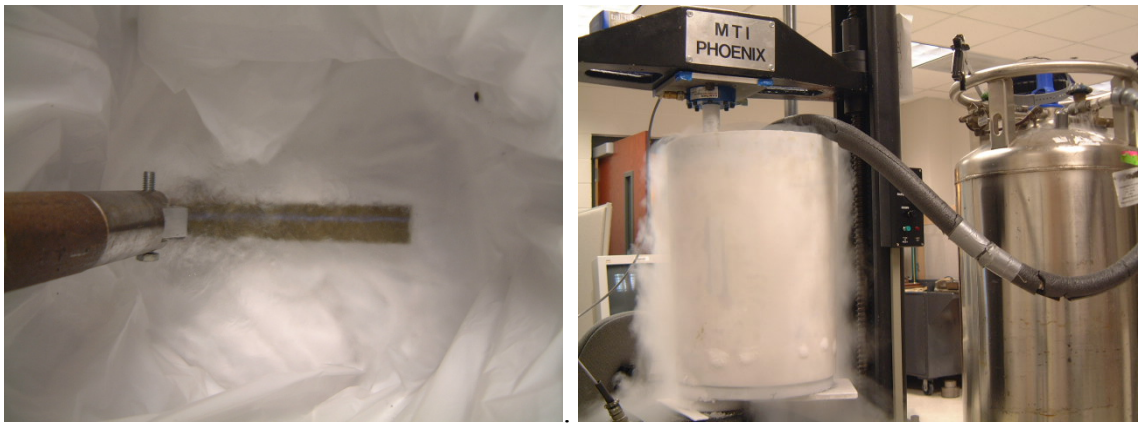

Figure 2.10 Specimen in liquid Nitrogen and whole facility during cryogenic tests.

The deflection of the specimen was used as a guide to determine the point of unloading. After the deflection reached a certain value, the specimen was unloaded, as it was in room temperature tests. Then, the crack propagation length was measured by the same microscope after it was taken out of liquid Nitrogen.

Specimen Property Test

Carbon Fiber Face Sheet

As previously described, the curing method used for specimen preparation differs from the methods provided by Toray composites, (as provided in Appendix D.) Hence it is expected that the material properties would have been altered. The mechanical properties of the composite prepreg as reported by its manufacturer, Toray composites, Inc., are shown in Table 2.1. The material properties used in the present study are calculated by the methods that follow.

Table 2.1 Mechanical properties of composite prepreg provide by company.

Elastic modulus at laminar direction (E_1)	23.5 Msi
Elastic modulus at transverse direction (E_2)	1.1 Msi
Shear modulus (G_{12})	0.64 Msi
Poisson's ratio (v_{12})	0.34

Four-Point Bending Test at Room Temperature

There are several methods available for measuring the material properties of composite laminate. Three-point bending, four-point bending, tension, and compression tests are suitable for composite materials. In the present study, we chose the 4-Point Bending Test for measuring the elastic properties of composite laminates. It was thought that the four-point bending test would yield more accurate and repeatable results than the three-point bending test. Additionally, there would be no shear transverse shear force at the deflection of the mid-point. A small offset of the loading point, with respect to the whole setup, would not significantly affect the results.

The specimen dimensions are depicted in Figure 2.12. The stacking sequence of the specimen was $[0/90]_{2S.}$ The thickness of the laminate is 0.048 inch; and the width is about 1.0 inch, which has very small tolerance. Four different elastic properties (E_1, E_2, G_{12}, v_{12}) must be calculated to be used in FE analysis, therefore three-orientation specimens have been performed in the same test setup. The specimen with 0-degree orientation is for E_1, 90-degree is for E_2, and 45-degree is for G_{12}. Poisson's ratio is assumed to be unchanged with respect to temperatures. The tests are conducted under displacement control in a material testing machine at the rate of 0.05 in. /min. Load-deflection diagrams and test results are shown in Appendix E.

The elastic properties were calculated from the transformed lamina stiffness using the following formula [8]:

$$Ex = \frac{1}{\frac{1}{E_1}c^4 + \left[-\frac{2v_{12}}{E_1} + \frac{1}{G_{12}}\right]c^2 s^2 + \frac{1}{E_2}s^4} \tag{2,1}$$

where Ex is the transformed lamina stiffness with x degree determined by following the beam deflection theory:

$$\delta_{\max} = \frac{Pa}{24EI}(3L^2 - 4a^2) \tag{2,2}$$

where $P, \delta_{\max}$, respectively, is the load and the maximum deflection of the center, L is the total span, and loading point, a, is the distance from support. The inertia of moment (I) is calculated from geometry. To get specific deflections, all tests have been stopped when the mid-point of the specimen reached 0.45 inches from the initial position.

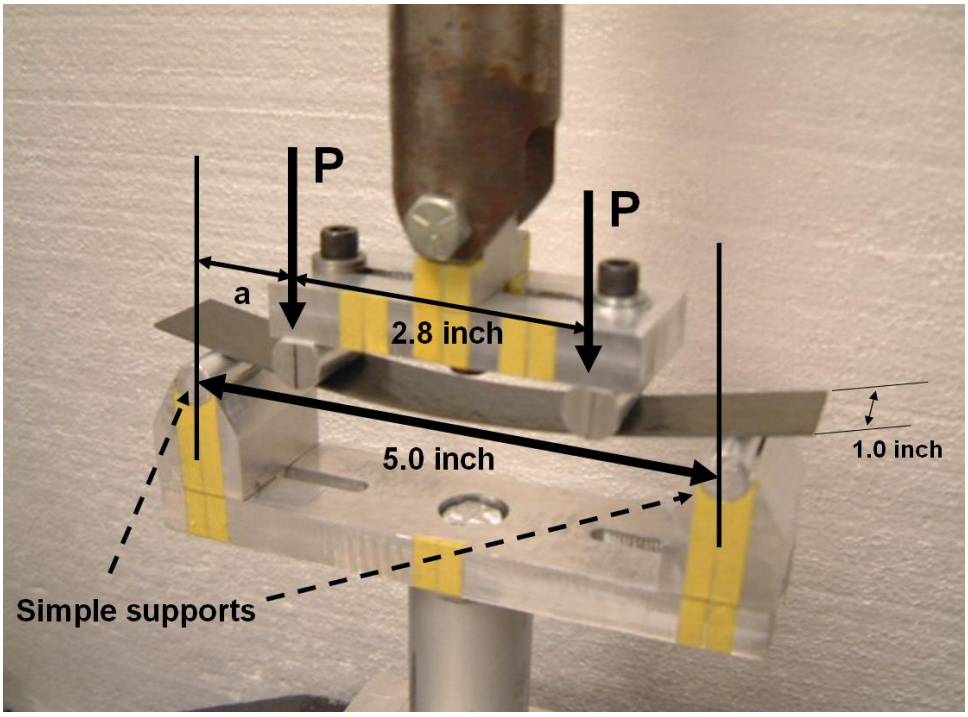

Figure 2.11 Specimen geometry and test setup of four point bending tests.

Table 2.2 Investigated material properties of tested composite laminates at room temperature.

Elastic modulus at laminar direction (E_1)	20.9 Msi
Elastic modulus at transverse direction (E_2)	1.16 Msi
Shear modulus (G_{12})	1.13 Msi
Poisson's ratio (ν_{12})	0.34

Four-Point Bending Test at Cryogenic Temperature

Ideally, for in-situ cryogenic testing, the coefficients of thermal expansion (CTE) should be known from the manufacturer. However, the company did not provide the CTE. The same test setup as room temperature tests was conducted to obtain the material properties at cryogenic temperatures; then was applied in FE analysis, shown in Chapter 4.

Also an in-situ cryogenic 4-point bending test was performed with the same test setup in a cryogenic chamber as described earlier in this chapter. The isothermal cryogenic test conditions at 77K were achieved by immersing the test specimen and loading the introduction apparatus into liquid nitrogen. In order to reach thermal equilibrium, the specimen stayed immersed in a constant level of the liquid Nitrogen for at least 30 minutes prior to mechanical loading.

The effects of cryogenic temperature on the modulus were found by examining the results from a specimen subjected to thermal condition. The $[0]_8$ laminate (E_1) experienced a slight (12%) increment in modulus at cryogenic temperatures. Similarly, the $[45]_8$ laminate for calculation of the shear modulus increased as the temperature decreased. In particular, the shear modulus increased by as much as 140% when tested at 77K. The transverse modulus (E_2) showed a slight incline at cryogenic temperatures, while the transverse modulus went up by approximately 65%, when the temperature was reduced to 77K. Lastly, Poisson's ratio was assumed to be unaffected with respect to thermal conditions. Load-deflection graphs related to cryogenic temperatures are presented with room-temperature test results in Appendix E.

Table 2.3 Investigated material properties of tested composite laminates at cryogenic temperature.

Elastic modulus at laminar direction (E_1)	23.4 Msi
Elastic modulus at transverse direction (E_2)	1.92 Msi
Shear modulus (G_{12})	2.71 Msi
Poisson's ratio (ν_{12})	0.34

At the same time, material properties from experimental analysis were verified through FE analysis. The commercial FE program, ABAQUS is used to make a 2D solid model of the test setup and specimen. After running a program with material properties in Table 2.2 and 2.3, the mid-point deflection of the specimen showed very good agreement with the experimental results.

Figure 2.12 In-situ cryogenic 4point bending test in liquid Nitrogen.

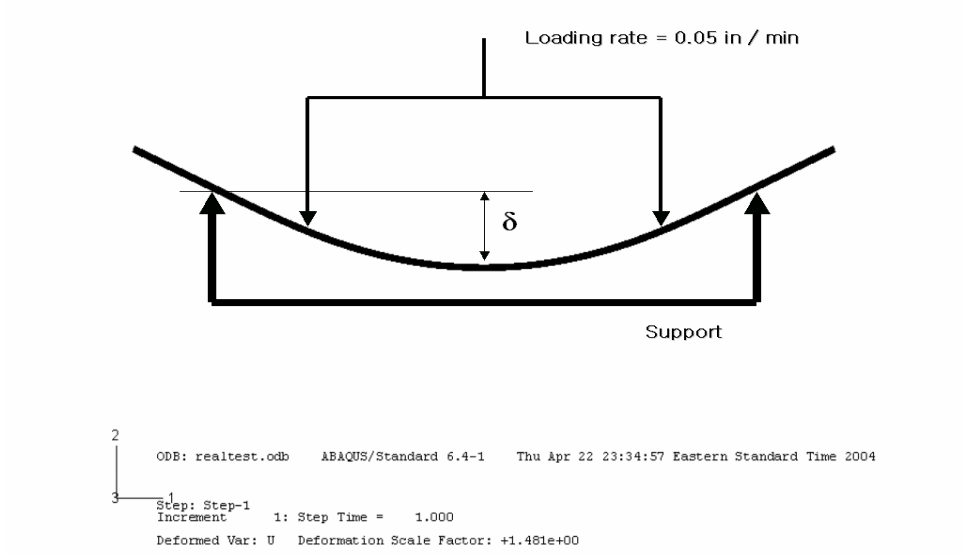

Figure 2.13 2D model of test setup and specimen.

Honeycomb Core Material

For honeycomb material property, mechanical properties are generally determined the following: peak and crush compressive strength, crush compressive modulus, L and W plate shear strengths and moduli. For energy absorption applications the crush strength is needed, which is approximately 50% of the bare compressive strength. All of the honeycomb manufacturers provide brochures containing their core product's properties. It is assumed that the material properties of honeycomb could be the same at both room and cryogenic temperatures.

The Poisson's ratio of a material is the ratio of the lateral strain to the axial strain where the strains are caused by uni-axial stress only. Generally it is in the range of 0.15 to 0.35. In extreme cases, values as low as 0.1 (concrete) and as high as 0.5 (rubber) occur. The latter value is the largest possible.

Table 2.4 Honeycomb properties of 2D model in ABAQUS

Elastic modulus at L direction at T direction	1000 psi 30000 psi
Shear modulus at LT direction at LW direction at WT direction	10000 psi 100 psi 5000psi
Poisson's ratio	0.1

For normal materials a tension or compression test is conducted measuring the lateral and axial deformations. In addition the Poisson's ratio is calculated. This does not work for honeycomb. If the honeycomb core is compressed, the cell walls can buckle inward or outward. Also, one side can go in and the other out. In some FE programs the Poisson's ratio of material must be entered or the program will not run. Usually the honeycomb core moduli are so much smaller than the facings that it does not matter what

honeycomb Poisson's ratio value is assumed. The core just moves with the facings, offering almost no resistance. The in-plane honeycomb properties are almost zero and would offer little resistance. Perhaps the best method is to use a honeycomb Poisson's ratio of 0.1 in the FE program, then use 0.5 and see if there is any difference in the results. This will show the program sensitivity to the honeycomb Poisson's ratio.

Summary and Conclusion

With three different orientations at room temperatures and cryogenic temperatures, six composite laminate specimens have been examined to evaluate elastic modulus. The cryogenic chamber is created for tests at 77K. The research related to the thermal dependent properties is not available from the manufacturers so the specimens must be tested to determine property variations with respect to temperature. In a four-point bending test, as temperature is reduced, the modulus of all the laminates increased. The notable increase in elastic property occurs in the G_{12}.

CHAPTER 3
FRACTURE TOUGHNESS TEST

Double Cantilever Beam (DCB) Tests

Most of the important interface fracture problems involve combinations of normal and shear forces along the crack, such that "Mixed Mode" conditions prevail. Now for clarification and completeness it is necessary to understand the differences in loading modes and how they are defined. There are three loading modes in fracture mechanics; Mode I, Mode II and Mode III. Mode I is dominated by opening load, Mode II is dominated by in-plane shearing load, and Mode III is done by out-of-plane load.

Mixed mode conditions are possible when two or more loading conditions are present. Generally, in any bulk material, a crack will propagate in the direction that minimizes the mode component of loading. However, in constrained or interfacial loading, the crack can propagate such that the mode I and mode II components are both significant. Mixed mode conditions are quantified by a mode mixity phase angle ψ, which is 0° for pure mode I and 90° for pure mode II. Understanding the mode mixity of a loading condition is important because of its effects on crack propagation.

$$\psi = \tan^{-1}\left(\frac{K_{II}}{K_I}\right) \tag{3.1}$$

Fracture at interfaces between dissimilar materials is a critical phenomenon in many systems, ranging from composites to microelectronic devices. However, both the fundamental mechanics of this process and experimental techniques capable of

systemically characterizing such fracture are incompletely developed. The principal intent of the present paper concerns the development of a test procedure for purpose of systematic measurement of the interface fracture resistance.

It should be noted that the DCB test is usually performed in mode I fracture studies but experiments on asymmetric DCB specimens should provide the same data as other mixed mode tests. This study is performed by using asymmetric DCB loading, with three-core thicknesses at room and cryogenic temperatures. The recorded data and calculated values are listed in Appendix B and C. However, it is not possible to calculate the phase angle for mixed mode conditions with this data, because the experimental data represents the global behavior. A detailed FE analysis is required in order to understand the local crack tip stress behavior and hence to determine the mode mixity.

DCB Tests at Room Temperature

The energy release rate was calculated from the experimental data. The load and displacement values were obtained during the fracture test. The energy released for a given extension is the area under the load-displacement curve. Examples of the areas used for unsteady and steady crack growth are shown in Figure 2.9. The area is calculated under each loading-unloading cycle.

The area of the graph, ΔE, corresponds to the energy-released as the crack grows. The critical energy release rate or fracture toughness (G_c), was obtained using

$$G_c = \frac{1}{b}\frac{\Delta E}{\Delta a} \tag{3.2}$$

In this expression, ΔE is the area calculated from the trapezoid rule, Δa is the crack extension noted during the test, and b is the width of the specimen. The value calculated

is the average energy released for the crack extension, Δa. The procedure was repeated for each loading/unloading cycle or between indicated critical load values. Hence, several values were obtained from a single test specimen. The method was repeated for specimens of various thicknesses.

Average G_c values were calculated using Equation 3.2, disregarding the first few cells of crack propagation where the non-porous Teflon is put in the sandwich composites to make pre-existing cracks. When fabricating the test specimens the initial crack tip will likely look and behave differently compared to subsequent cracks created by the natural crack propagation. It should be noted that, when making an artificial crack, the radius of the crack tip will be finite depending on the thickness of the material used to prohibit bonding of the crack surfaces. Therefore, how the crack was formed affects the state of stress and the fracture toughness. We anticipated disagreement in the results from the first crack propagation when compared to those of subsequent crack propagation. Due to the effect of cells on the first crack of the specimen, Figure 3.1 and Figure 3.2 show the difference of average G_c. The average of G_c is given in Table 3.1.

Table 3.1 Average G_c for different core thickness with and without the initial crack data. The Coefficient of Variation is given in parenthesis.

Core Thickness (inch)	0.25	0.5	1.0
Average (lb./in.) w/ 1st crack data	2.93 (22.3%)	2.04 (38.7%)	1.64 (39.9%)
Average (lb./in.) w/o 1st crack data	3.27 (11.8 %)	2.3 (21.1 %)	1.49 (44.3 %)

The effect of including and excluding the data from initial crack propagation is shown in Fig. 3.1.

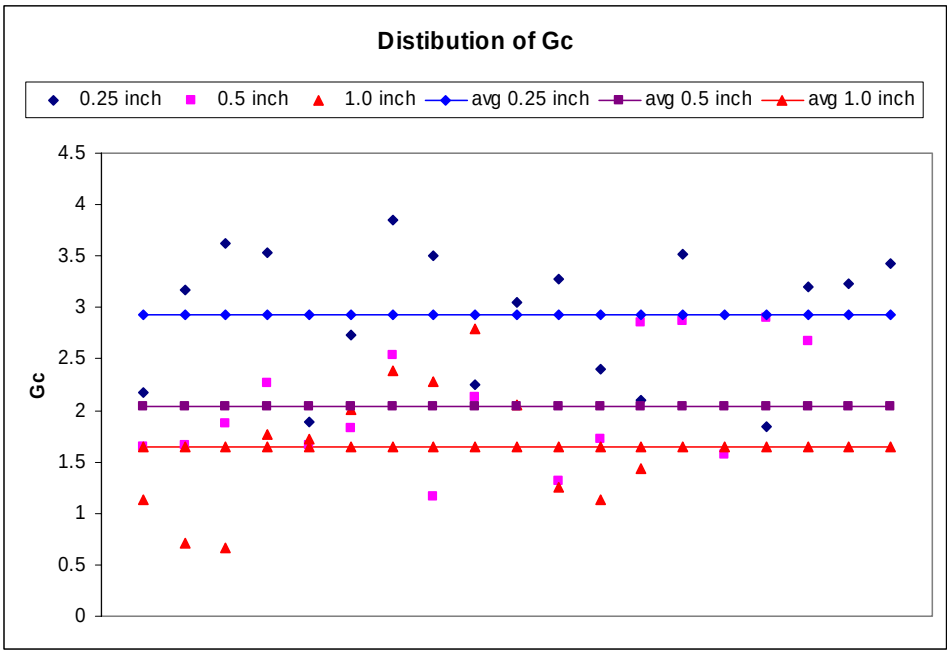

Figure 3.1 Distribution of fracture toughness and average values with variation of core thickness.

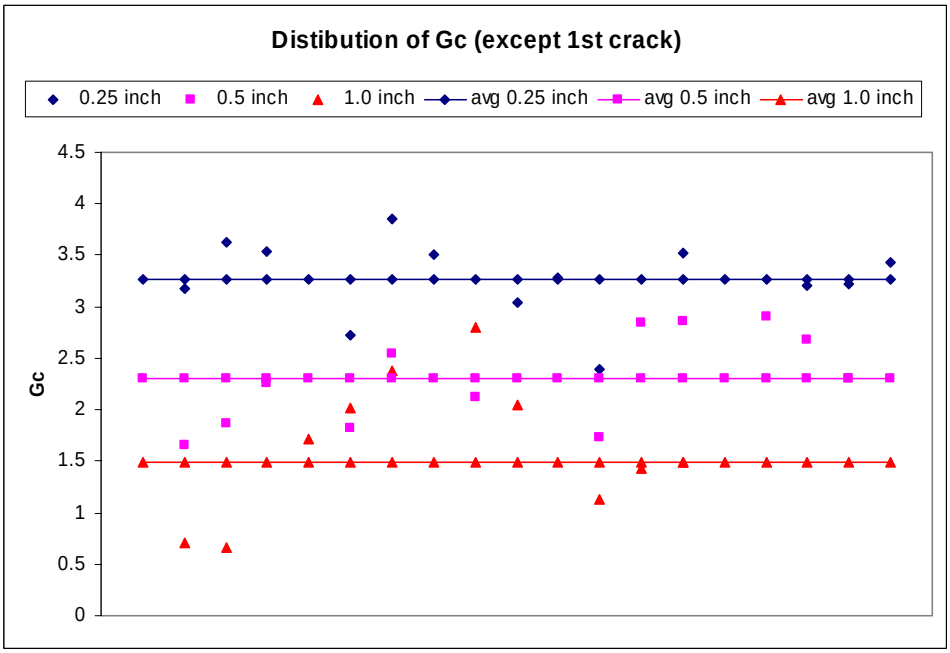

Figure 3.2 Distribution of fracture toughness and average values with variation of core thickness excluding 1st crack propagation data of each specimen.

The experimental data were analyzed to understand the effects of core thickness and crack length (R-Curve effect) on the fracture toughness. Figure 3.3 shows that the

variation of fracture toughness as a function of crack length for different core thicknesses. A linear fit was used to curve-fit the data.

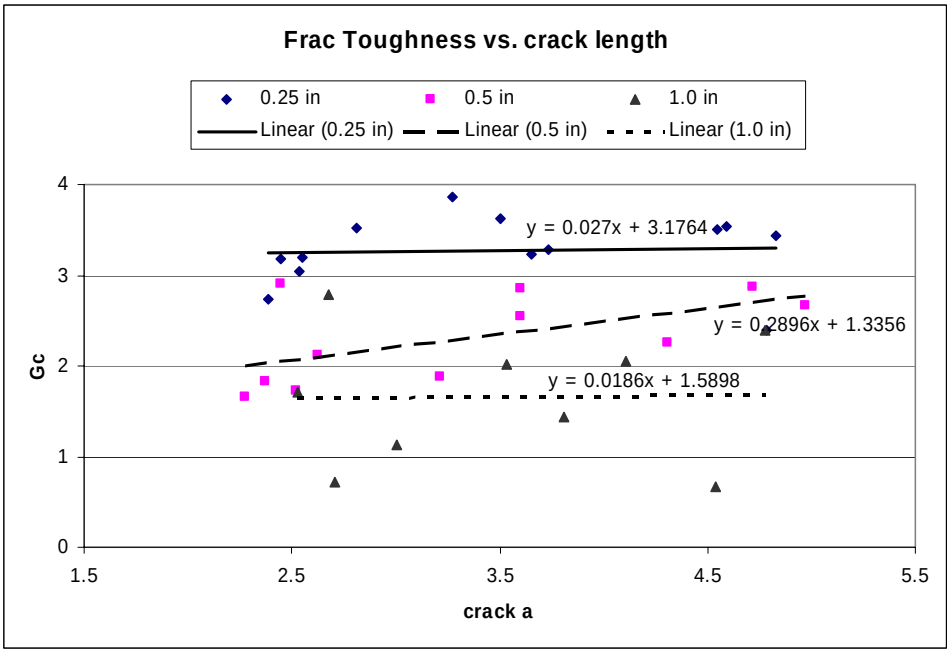

Figure 3.3 Trend lines and all data of fracture toughness vs. crack length.

A statistical analysis was conducted on the experimental data to calculate the average G_c. Initially all data of the specimens were plotted separately and compared to consider a general trend of core thickness affecting fracture toughness. Figure 3.4 illustrates the trend of fracture toughness vs. core thickness from experimental data, excluding the first crack data of the specimen. Good consistency is shown in a decreasing fracture toughness G_c vs. an increasing core thickness, when reviewing the data having core thickness 0.25 in, 0.5 in and 1.0 in.

Therefore, it is logical to say that, even though there is a slight discrepancy within data, core thickness for honeycomb sandwich composites indeed affects the critical fracture toughness at an inversely proportional rate.

DCB Tests at Cryogenic Temperature

The aim of this study is to understand the failure phenomena of the sandwich composites under cryogenic conditions.

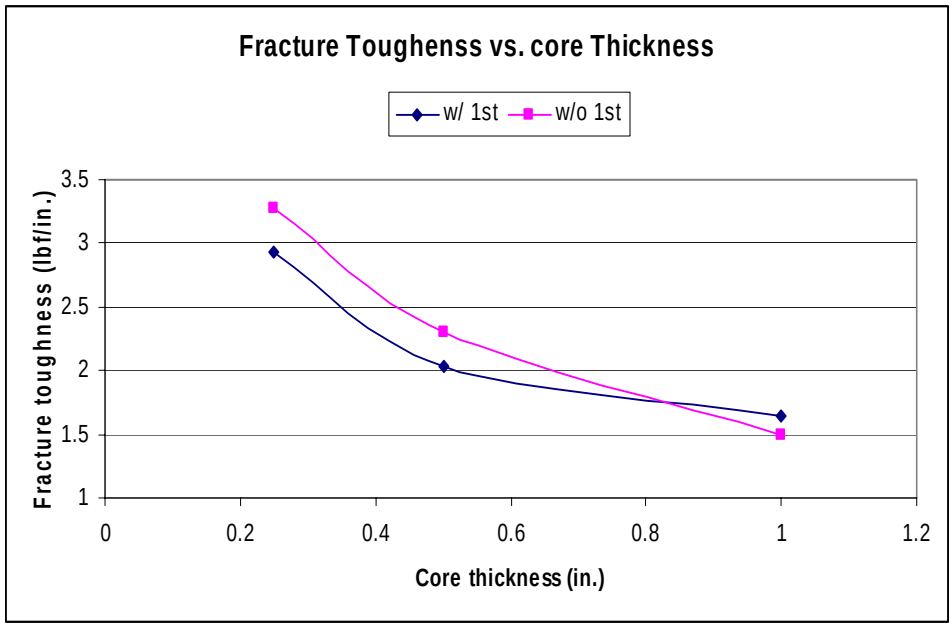

Figure 3.4 Slope of fracture toughness according to core thickness.

To investigate the effect of cryogenic temperatures on the fracture toughness of sandwich composites, the DCB tests described in Chapter 2 were performed in liquid Nitrogen at 77K. It is not possible to see the crack propagation in cryogenic tests because the specimen is immersed in liquid nitrogen in an insulated vessel. Hence, the deflection of the specimen is used as a guide to determine the point of unloading. After the opening displacement reaches a certain value, the specimen is unloaded as in room temperature tests. In manufacturing the specimen, a cryogenic adhesive is used to bond the loading tabs to the face-sheets. During tests, M/S Epoxy 907 was first used to bond the face sheets and tabs, but proved that general adhesive is not useful at cryogenic temperatures. Therefore a special cryogenic adhesive was applied to tests at cryogenic temperatures.

Except bonding, most test setups and procedures were the same as at room temperature. The same equation was applied to get the energy release rate at cryogenic temperatures with test data excluding the first crack data. Cryogenic test data is listed in Appendix C, and the calculated fracture toughness G_c, based on three-different thicknesses, are shown in Figure 3.4, with those at room temperature. Figure 3.5 shows the degree to which fracture toughness dropped at cryogenic temperatures, compared to room-temperature data.

Table 3.2 Experimental investigated fracture toughness at room temperature and at cryogenic temperature.

Temperature	Room			Cryogenic		
Thickness	0.25	0.5	1.0	0.25	0.5	1.0
Experimental G_c	3.27	2.3	1.49	1.69	1.19	0.91

As shown in Figure 3.5, the fracture toughness drops by approximately 40 % at cryogenic temperature and the fracture toughness decreases with increasing core thickness as in the case of room temperature tests.

Four-Point Bending Tests

Most of the important interface fracture problems involve combinations of normal and shear forces along the crack, such that “Mixed Mode” conditions prevail. As will be seen later the DCB tests yield conditions where in the mode mixity ranges from 10 deg. to 25 deg. In order to obtain fracture toughness at larger angles, e.g., 50-60 deg. range, a different specimen is needed. An appropriate specimen is depicted in Figure 3.6, consisting of a notched, bimaterial flexural beam. It will be demonstrated that this

specimen provides fracture results for conditions of approximately equal normal and shear forces in the interface crack far from the tip.

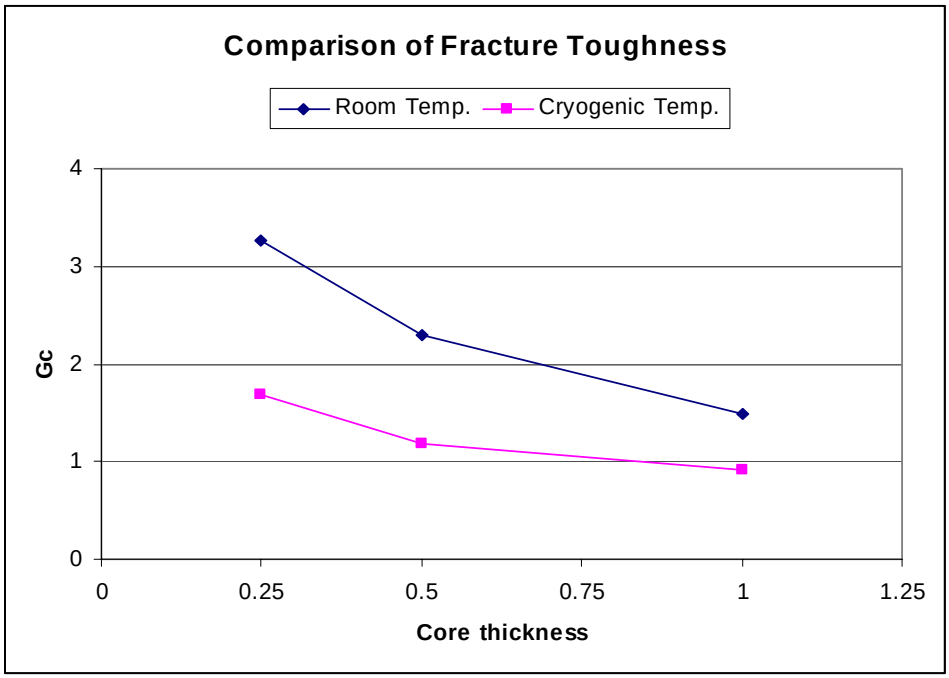

Figure 3.5 Comparison of experimentally investigated fracture toughness at room temperature and at cryogenic temperature.

Consequently, when used in conjunction with other specimens, fracture resistance data can be obtained for a range of mixed mode conditions.

Charalambides et al. [10] evaluated the utility of the flexural specimen in Figure 3.6 for determining the interfacial fracture toughness of aluminum/PMMA bi-material specimens. Specifically, laminates of these materials have been bonded with an initial interface crack created by placing a small piece of non-porous Teflon along the interface, at the center of specimen prior to bonding. The interfacial crack propagations from the initial crack on loading are averted by causing controlled extension of the crack prior to testing. Crack lengths monitored from the displacement movement of MTI are independently checked by means of direct optical observations of the front crack.

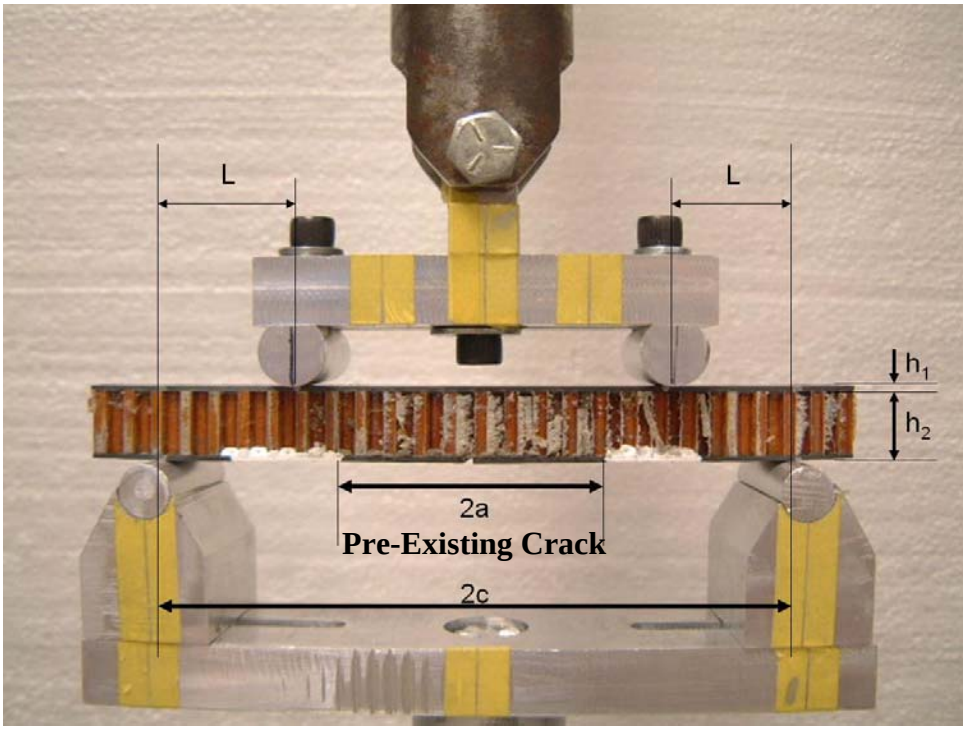

Figure 3.6 Notched four-point bending specimen with asymmetrical interfacial cracks.

In this research, the same method was tried to estimate the interfacial fracture toughness of honeycomb core sandwich specimens. Four-point bending tests for fracture toughness have generated a greater phase angle than in asymmetric DCB tests [10]. By considering this bending test and DCB test at the same time, the fracture toughness of asymmetric bimaterial sandwich systems can be investigated for a wide range of mode-mixity.

However, the shear strength of the honeycomb material is much less than the interfacial bond strength. Hence before the crack could propagate the core fails as shown in Figure 3.7. In Figure 3.8, it is very difficult to check which point is the critical load at the beginning of the crack-tip because there is no sudden load drop in the diagram. Hence it is concluded that the aforementioned specimen is not suitable for sandwich specimens with a highly flexible and weak core material.

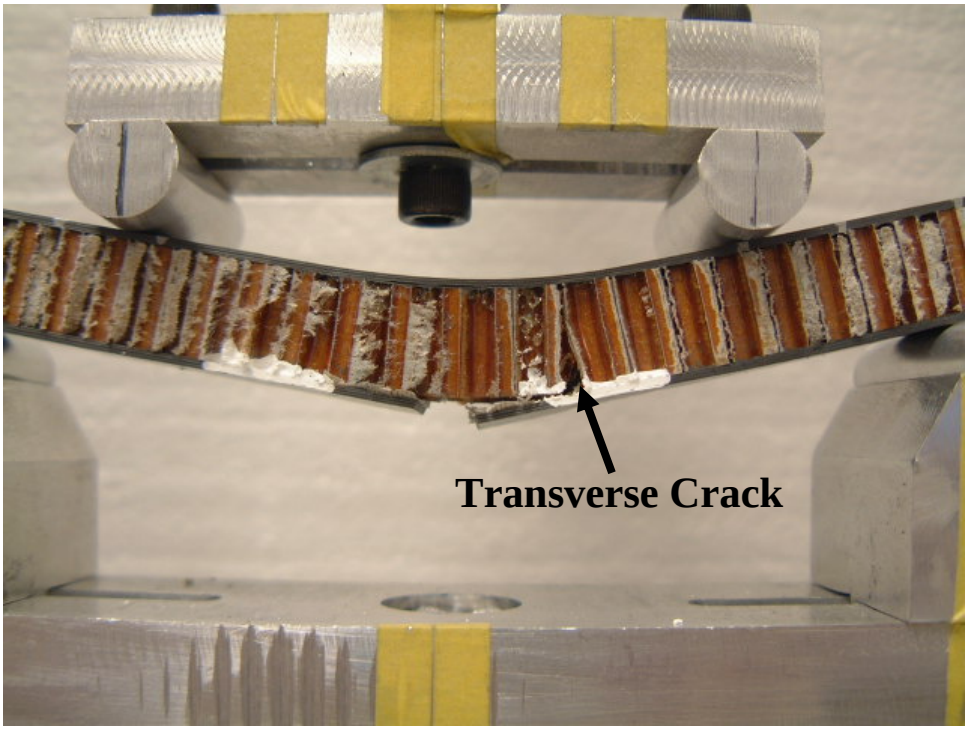

Figure 3.7 Transverse crack made during 4-point bending tests.

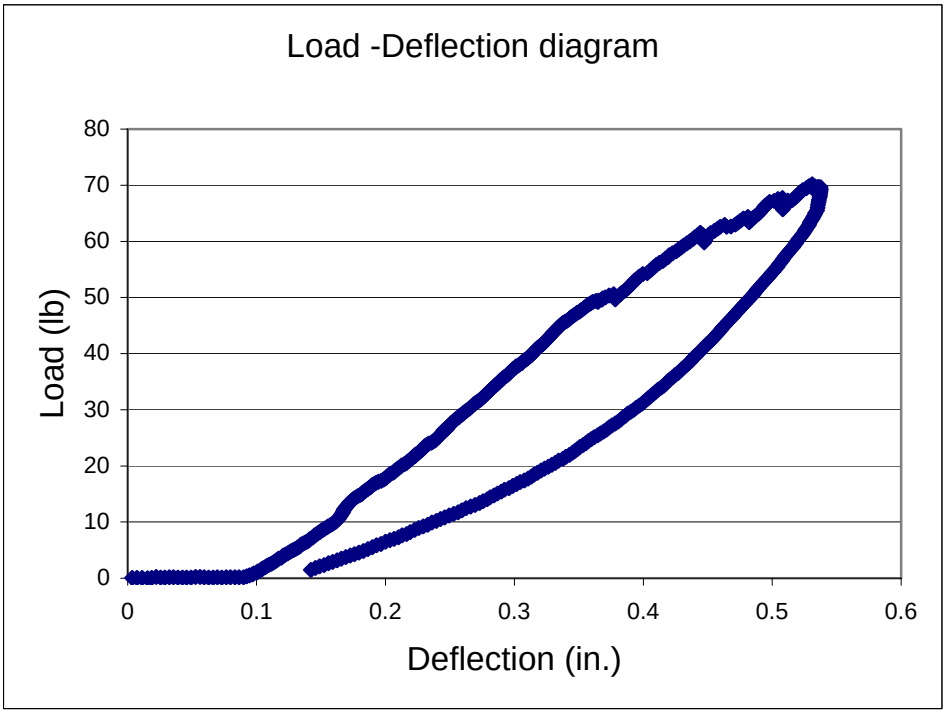

Figure 3.8 Example diagram of 4-point bending flexural test with center-cracked sandwich specimen.

Summary and Conclusion

Sandwich composites of carbon/face-sheets and honeycomb cores were tested to estimate their fracture toughness at room temperature and at 77K in liquid Nitrogen (cryogenic temperature). A specialized fixture and test procedure were developed for testing at cryogenic conditions. The resulting load-deflection diagrams were used to estimate the interfacial fracture toughness using the area method. First, an asymmetric specimen was tested at two different temperatures: room temperature and cryogenic temperature with three different core thicknesses. It is shown that fracture toughness drops significantly at cryogenic temperatures. This should be a factor in using the sandwich composite system in liquid Hydrogen tanks.

Moreover, as a core thickness gets thinner, fracture toughness increases. So, in sandwich systems, core thickness could be considered as one significant factor dominating fracture toughness.

On the other hand, even though four-point bending tests were performed with the same sandwich composites, this did not produce any valid results. Due to the low stiffness and strength of the honeycomb core, the transverse crack occurred in the specimen. Therefore the four-point test method is not suitable for such specimens. However, it was anticipated that the four-point bending test would yield a higher range of fracture toughness and mode-mixity.

In the next chapter the FE model used to estimate the mode-mixity in the test specimens are described. The purpose of the FE analysis is that the fracture toughness can be correlated with mode-mixity rather than core thickness.

CHAPTER 4
FINITE ELEMENT ANALYSIS

In structures, damages may be detected by using a number of sophisticated techniques or by viewing visible deformation. Damage in composite structures is rarely visible, and non-destructive evaluation often does not detect certain forms of damage. These undetected cracks can result in the failure of the component, incurring loss of human life, damage to machinery, or reduced equipment life. The study of the initiation and growth of cracks is termed “fracture mechanics”.

Laminated composites are susceptible to flaws that develop in the interface region between laminated plies [9]. Such flaws are referred to as “delamination” and can develop from a host of root causes that range from manufacturing defects to low-energy impact. Delaminations of this type lead to degradation in the load carrying ability of the structure and under certain conditions can lead to catastrophic failure of a structural component. Composite sandwich structures can fail in much the same way. It is common for flaws to develop at the interface of the face-sheet and the core. In sandwich materials with an open-celled core, such as a honeycomb core, this happens in the adhesive layer, and the skins can peel away from the core. This is termed “interfacial failure” and stems from the interfacial crack.

When a crack is present in a load bearing structure, there are three-modes of fracture that may occur simultaneously. They are: opening mode (Mode-I), sliding or in-plane shearing mode (Mode-II), and tearing or out-of-plane shearing mode (Mode-III), (shown in Figure 4.1). In general, all three modes exist for a flaw in a structure subjected

to complex loading. However, in some instances, Mode-I, Mode-II or Mode-III, combinations of two modes may exist. In this study time-dependent behavior (fatigue) and Mode-III are not considered.

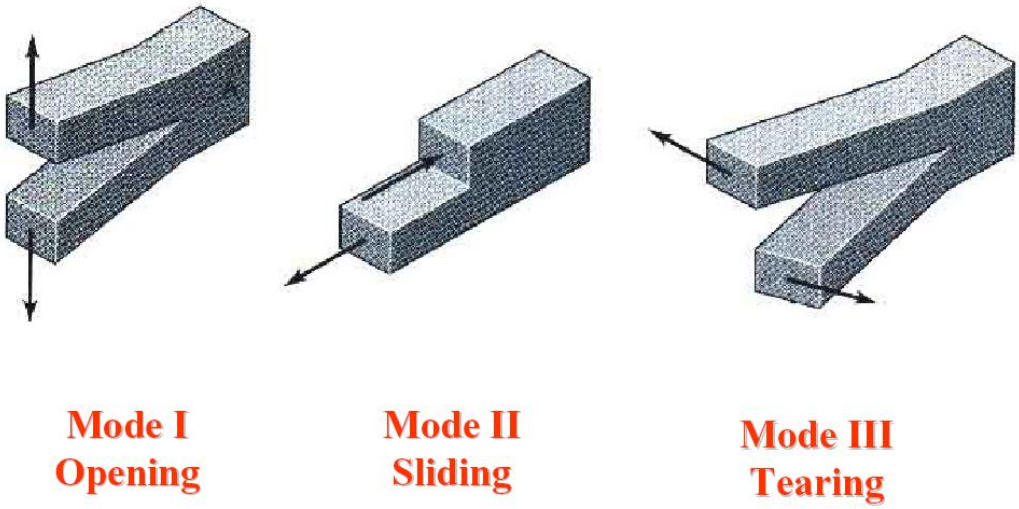

Figure 4.1 Crack displacement modes.

Modeling

In the preceding discussion [1], analytical expressions are shown that can be used to evaluate fracture toughness in sandwich composites. These analytical expressions are useful because they show a methodology that can be used to evaluate the fracture of more complex configurations. Unfortunately, exact analytical expressions do not exist for all crack configurations. Numerical techniques must be used to evaluate the fracture parameters for these configurations. The most common numerical method used to evaluate structures is FE modeling. Several techniques to evaluate the crack tip stress fields in cracked solids have been developed based on FE analysis. Methods exist for the evaluation of fracture parameters using forces and displacements obtained from a FE analysis. As noted previously, to predict fracture toughness, a critical value of the stress

intensity factor (SIF) must be known. This is compared to the local state of stress in a cracked solid. Fracture occurs when the local value reaches the critical value. Critical values of fracture toughness or the stress intensity factor are developed from fracture testing. Hence, in order to evaluate fracture toughness in the sandwich material, a computational model must be developed for the cracked material. Both the stress intensity factor (SIF) and the phase angle (ψ) can be determined from these models.

Typical elastic moduli of face-sheets and core material are investigated as described in Chapter 2, and assumed for the transversely isotropic layer. For the present analysis, FE models are constructed with the commercial code ABAQUS using 2D 4-node bilinear, reduced integration with hourglass control. The FE models are designed using the experimental setup as a base. The face-sheets are separated into individual layers of 0 and 90 degrees with the properties given in Chapter 2. Three core-thickness models, 0.25, 0.5 and 1.0 inch, are created for determining the mode mixity. Figure 4.1 represents schematically the 3D model loading and boundary conditions: lower edge displacements in the x and z directions are restricted, z-direction displacement is applied to the upper edge, i.e. u=0 [11]. Figure 4.2 shows a typical FE mesh including a zoom-in view of the vicinity of the crack tip zone. For high accuracy, the area of 0.012 inch × 0.012 inch around the crack tip is represented by 1600 elements with radial mesh. Away from the crack tip, bigger elements have been made to avoid excessive computational cost. Crack length and applied load can be determined from experimental data for use in all models.

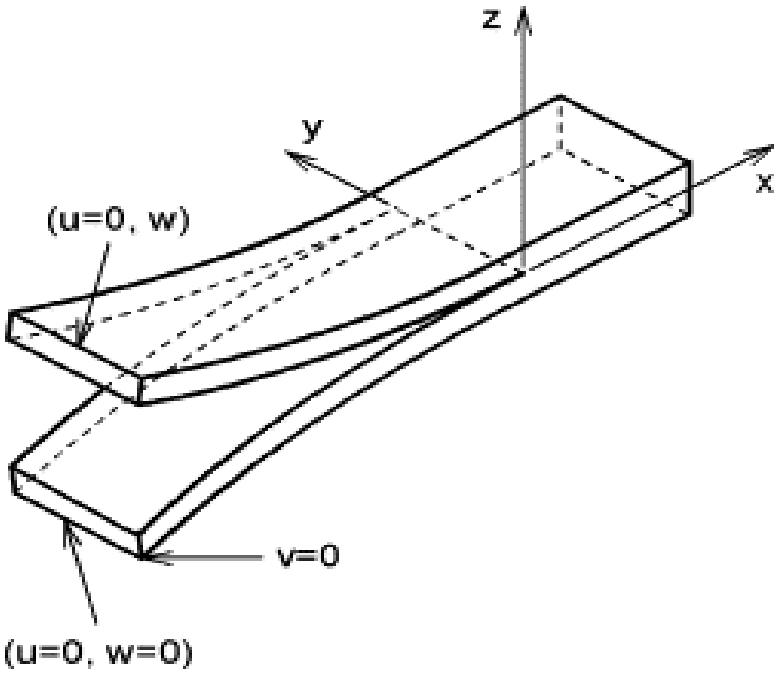

Figure 4.2 Schematic view illustrating the model loading and boundary conditions [11].

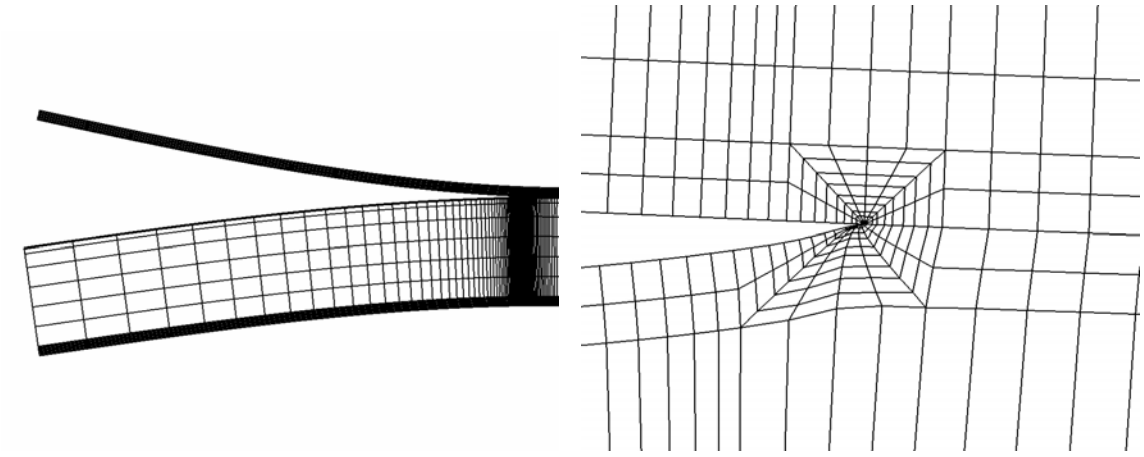

(a) (b)

Figure 4.3 FE models of the sandwich specimen; (a) Plane (two-dimensional) solid model, (b) Radial FE mesh in the vicinity of the crack tip.

Therefore, it is decided that the experimental critical load can be used in the model and the crack length should be checked to match deflections from experimental tests and FE modeling. The critical load as related to deflection value, the experimental fracture

toughness (G_c) and the average of the G_c value for given core thicknesses of the modeled specimens are given in Appendices B and C.

Moreover, to verify the validation of this two-dimensional model, three-dimensional analysis has been executed simultaneously. The same critical load was applied in both models and then the deflection in the out-of plane direction at the end of the specimen is compared. Both deflections were found to be nearly the same; therefore the 2D model in this paper is proven to be valid, and will be used in subsequent analyses.

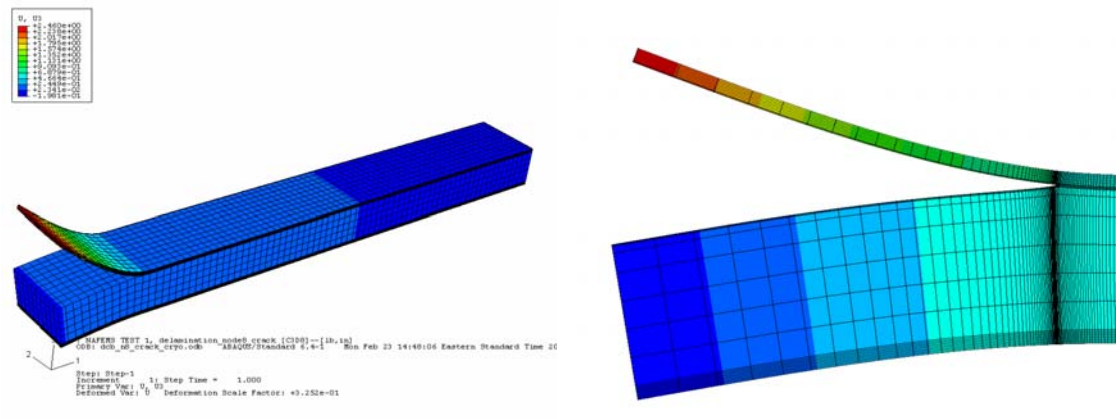

(a) (b)

Figure 4.4 FE models of the sandwich specimen; (a) Three-dimensional model, (b) Plane (two-dimensional) solid model.

Analysis

The FEM (finite element modeling) in this paper is performed by applying loads as measured experimentally and then comparing resulting crack lengths and fracture toughnesses. Numerical results are listed in Appendix B and C. Material properties are shown Tables in Chapter 2.

ABAQUS has the specific command for fracture toughness, “CONTOUR INTEGRAL”, which can yield the *J*-Integral value in the data, which is equal to the energy release rate in a linear elastic body. In this analysis, *J*-Integral from FEM can be

considered as fracture toughness (G_c) when the experimental fracture load is applied. The comparison of values is given in Table 4.1, and shown in Figure 4.3.

Table 4.1 Comparison of fracture toughness between from experimental and from FEM according to core thickness and temperature.

	Thickness	Experimental G_c	FEM *J*-Integral
Room Temperature	0.25	3.27	3.3
	0.5	2.3	2.13
	1.0	1.49	1.45
Cryogenic Temperature	0.25	1.69	1.81
	0.5	1.19	1.2
	1.0	0.91	0.98

As provided in Table 4.1, the difference between FE analysis and experimental results is less than 10 % for both room temperatures and cryogenic temperatures. *J*-Integral also dropped significantly, by about 50%, at cryogenic temperature, as much as fracture toughness did at the same thermal condition.

Next, investigation of phase angle for mixed mode and fracture toughness of sandwich composites, which is considered as a bimaterial system, was performed. For this analysis, the stress intensity factor for mode I and mode II is calculated from the results of the FE solution.

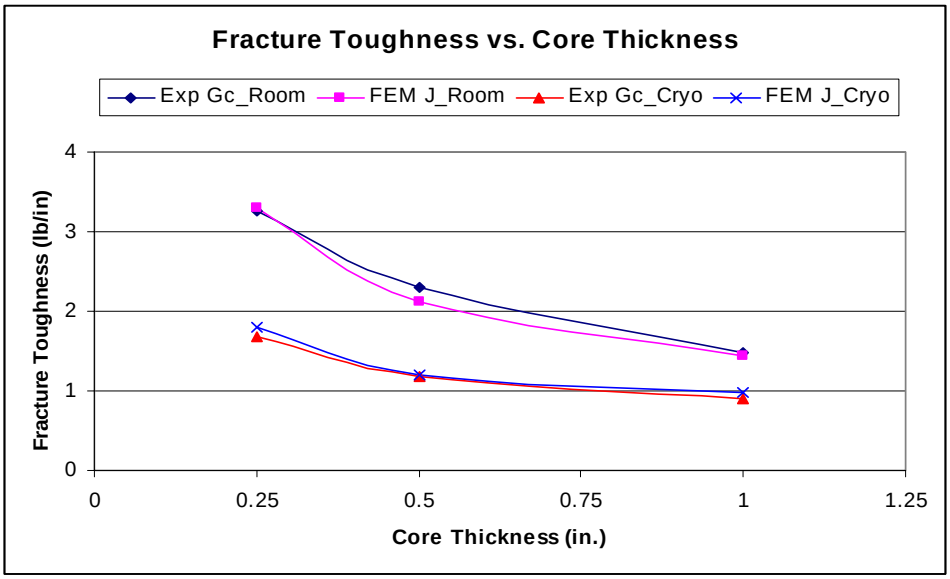

Figure 4.5 Plot of fracture toughness between from experimental and from FEM according to core thickness and temperature.

Calculations of fracture toughness and the stress intensity factor in dissimilar anisotropic media were discussed by Suo [7], and the results are provided in the Appendix. First, the bimaterial parameters, ε, λ and β are calculated at room and cryogenic temperatures, using MATLAB. The values are shown in Table 4.2. Equation (A.13) is used to obtain H_{11} and H_{22} and values of normal stress and shear stress in the vicinity of the crack tip can be obtained from the output data of the 2D FE model solution. Thus fracture toughness of sandwich composites can be obtained from Equation (A.14) which is rearranging Equation (A.11), (A.12) and (A.13).

Table 4.2 Calculated parameters for bimaterial media by MATLAB coding.

Temperature	H_{11}	H_{22}	β	E
Room	0.0011	1.98e-4	0.1781	-0.0573
Cryogenic	0.0011	1.9765e-4	0.1784	-0.0574

With parameters in Table 4.2 and local stresses from ABAQUS, the energy release rate and stress intensity factors are calculated using Equation (A.13) and (A.14). Consequently, the phase angle for mode-mixity can be known from Equation (A.15). The calculated results are listed in Table 4.3.

Table 4.3 Fracture toughness and phase angle.

Temp.	Thickness	Exp. G_c	FEM J Integral	G_c by Suo	Phase Angle
Room (296 K)	0.25	3.27	3.3	3.6	14
	0.5	2.3	2.13	2.11	18.7
	1.0	1.49	1.45	1.46	18.1
Cryogenic (77 K)	0.25	1.69	1.81	1.9	13.9
	0.5	1.19	1.2	1.17	19.1
	1.0	0.91	0.98	0.95	19.2

Figure 4.4 shows the consistency of fracture toughness reduction as the core thickness increases and also at cryogenic temperatures. For each case, in both in experimental results and the FE results, the G_c values decrease by the same portion. Good agreement is shown among three methods to calculate fracture toughnesses: the experimental area method, the *J*-Integral by ABAQUS and Suo's equation considering bimaterial media.

Fracture toughnesses at cryogenic and room temperatures have been investigated using three methods. Those values at cryogenic temperature are smaller than those at room temperature by approximately 40 %. When core thickness increases, fracture toughness decreases.

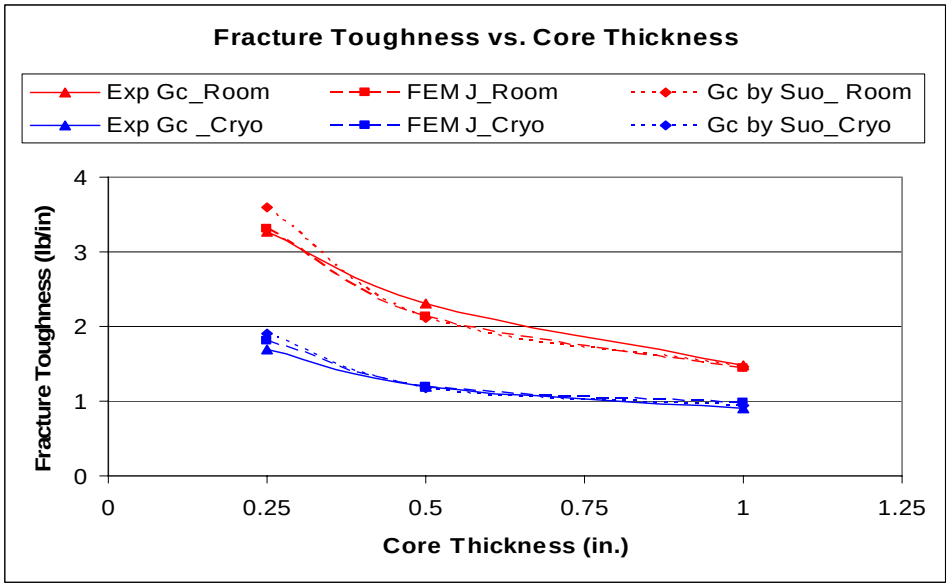

Figure 4.6 Fracture toughness at room temperature and at cryogenic temperature according to core thickness.

The mode-mixity values summarized in Table 4.3 also vary according to core thickness and temperature decline. Assuming that the phase angle of a sandwich composite with a 0-inch core thickness is close to zero, and then all phase angles for mode-mixity are shown in Figure 4.7.

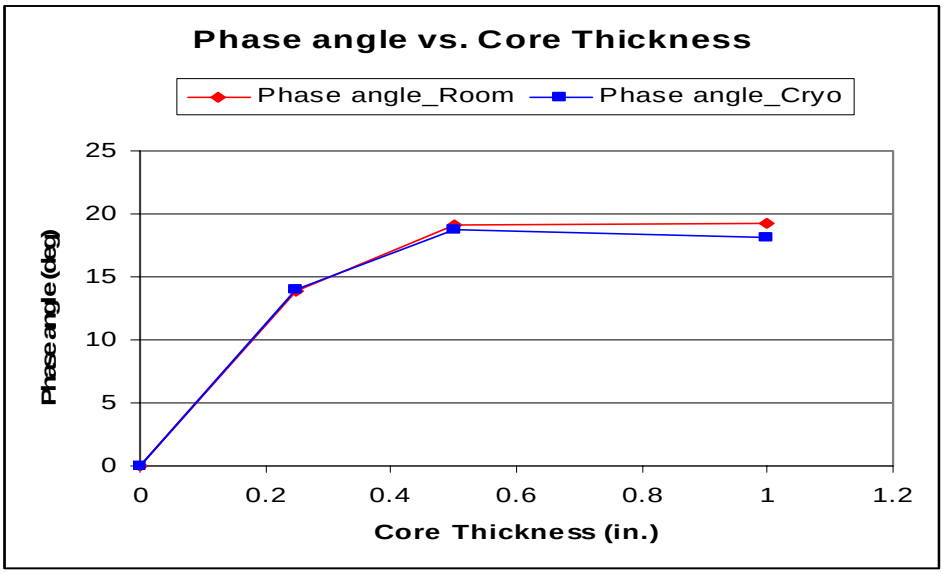

Figure 4.7 Phase angle for mixed mode at room temperature and cryogenic temperature.

Consequently the values of the phase angle are within the range, $0 < \psi < 20$. As core thickness increases, the phase angle also increases. Since the test setup is a modification of DCB (an usual test method for Mode I), the range of the phase angle is in the lower degree values, less than 20 degrees.

Summary and Conclusion

ABAQUS has been used to obtain the *J*-integral values directly from the data file. The stress intensity factor was calculated in order to be able to evaluate the fracture toughness and mode-mixity. FEM analysis has very good agreement with the experimental data, within less than 10 percent difference. The equations for a bimaterial system are used to do this analysis.

However, even though temperature has been assumed to affect the mode-mixity of sandwich composites, which seemed to be a factor of fracture toughness, it did not produce significant difference. More investigation should be executed to prove the relationship between mode-mixity and fracture toughness.

CHAPTER 5
CONCLUSIONS

Conclusion

Fracture toughness tests, similar to DCB tests, are performed on sandwich panels containing initial delaminations. The fracture toughness is measured for various crack lengths. The loads at which crack propagation occurs are applied in the FE model of the panel to obtain the detailed stress field in the vicinity of the crack-tip.

With three different thicknesses both room temperatures and cryogenic temperatures, six composite laminate specimens have been examined to evaluate elastic modulus. The cryogenic chamber was created for tests at 77K. Since the company manufacturing prepreg does not supply temperature dependent property data, the specimens must be examined to discover the change in material properties with respect to a significant drop in temperature. In a four-point bending test, as cryogenic temperatures reduced, modulus increased in all the laminates. The greatest increase in elastic property occurred in the G_{12}.

Sandwich composites of carbon/face-sheets and honeycomb core, were tested in critical loads and fracture toughnesses, at room temperature and at 77K in liquid Nitrogen (cryogenic temperature). A specialized alignment fixture and test procedure was developed for the cryogenic condition testing. First of all, an asymmetric specimen was tested at two different temperatures (room and cryogenic temperatures), with three different core thicknesses. Experimental test results were converted to fracture toughness using the energy-area method. It showed that fracture toughness drops significantly at

cryogenic temperatures. This should be a factor in using the sandwich composite system in liquid Hydrogen tanks.

Moreover, as a core thickness gets thinner, fracture toughness increases. So, in sandwich systems, core thickness can be considered as one important factor dominating fracture toughness.

Four-point bending tests were performed using the same sandwich composites in order to determine the fracture toughness at large mode-mixity angles. However, no valid results were produced. Due to the low stiffness and strength of the honeycomb core, transverse crack occurs in the specimen. So Equation 3.2 would not be valid for this test..

As expected, low temperature tests resulted in decreased values of *Gc*. This shows that the decrease in temperature leads to a more critical state for the material. Specimens showed sudden jumps during crack growth more frequently at cryogenic temperature than at room temperature.

In the FE model, the experimental critical loads were applied and the stress field in the vicinity of the crack tip was investigated. The FE analysis showed the degradation of fracture toughness resulting from cryogenic conditions.

ABAQUS was used to obtain J-integral values directly from the data. It also yielded the stress intensity factors that can be used to calculate the fracture toughness and mode-mixity. Fracture toughness of FEM analysis concurs closely with the experimental results within less than 10 percent difference. The equations by Suo for a bimaterial system were used to perform the analysis. It is expected that the results of this study will be important in the development of future material qualification methods and design of sandwich structures for cryogenic applications.

Suggestion for Future Work

1. One of the assumptions made was to consider a honeycomb core as a material in FEM analysis. However, honeycomb is not a material, but a structure from the micro-structural point of view. Future research should be carried out in consideration of honeycomb material as a structure, which consists of a wall structure and bonding material. This research could reduce the error of analysis in investigation of fracture mechanics with sandwich composites.

2. Another suggestion is to make a sandwich specimen using more layers of face-sheets. In this thesis, eight-layer laminates were used as face-sheets; so the difference in the variation of core thickness and temperature is changed slightly more than what is expected. If more lay-ups are used to make sandwich composites, it will be easier to check and compare analyses.

3. In order to determine the effect of larger values of mode-mixity on fracture toughness new test methods have to be developed such that the core does not tear before crack propagation. On the other hand tough core materials such as foam and balsa wood can be used in four-point bimaterial fracture tests in order to understand the effects of mode-mixity.

APPENDIX A
CRACKS IN DISSIMILAR ANISOTROPIC MEDIA

For a homogeneous material with *xy*-plane as a symmetry plane, the characteristic equation for in-plane deformation is [7]

$$l(\mu) \equiv s_{11}\mu^4 - 2s_{16}\mu^3 + (2s_{12} + s_{66})\mu^2 - s_{26}\mu + s_{22} = 0 \tag{A.1}$$

where μ are distinct complex numbers with positive imaginary part and s_{ij} are elastic constants in given orthotropic solids.

It has been shown by Lekhnitskii (1963) that the roots of an equation can never be real, and thus they occur in two conjugate pairs. Assuming they are distinct, one can choose two different roots, $\mu 1$ and $\mu 2$, with positive imaginary parts, to each of which a complex variable $z_j = x + \mu_j y$ is associated. The matrix *A, L, B* and *H* are 2 x 2, and the elements for *A* and *L* can be specialized from A.3 and A.4 with $\eta_1 = \eta_2 = 0$,

$$B \equiv iAL^{-1} = \begin{bmatrix} s_{11}\,\mathrm{Im}(\mu_1 + \mu_2) & -i(\mu_1\mu_2 s_{11} + s_{22}) \\ i(\overline{\mu_1}\,\overline{\mu_2} s_{11} - s_{22}) & -s_{22}\,\mathrm{Im}(\mu_1^{-1} + \mu_2^{-1}) \end{bmatrix} \tag{A.2}$$

The elements of the matrices *A* and *L* are given by

$$L = \begin{bmatrix} -\mu_1 & -\mu_2 & -\mu_3\eta_3 \\ 1 & 1 & \eta_3 \\ -\eta_1 & -\eta_2 & -1 \end{bmatrix} \tag{A.3}$$

and

$$A_{1\alpha} = s_{11}\mu_\alpha^2 + s_{12} - s_{16}\mu_\alpha + \eta_\alpha(s_{15}\mu_a - s_{14}), \tag{A.4.a}$$

$$A_{2\alpha} = s_{21}\mu_\alpha + s_{22}/\mu_\alpha - s_{26} + \eta_\alpha(s_{25} - s_{24}/\mu_\alpha), \tag{A.4.b}$$

$$A_{3\alpha} = s_{41}\mu_\alpha + s_{42}/\mu_\alpha - s_{46} + \eta_\alpha(s_{45} - s_{44}/\mu_\alpha), \tag{A.4.c}$$

for $\alpha = 1,2,$ and

$$A_{13} = \eta_3(s_{11}\mu_3^2 + s_{12} - s_{16}\mu_3) + s_{15}\mu_3 - s_{14}, \tag{A.4.d}$$

$$A_{23} = \eta_3(s_{21}\mu_3 + s_{22}/\mu_3 - s_{26}) + s_{25} - s_{24}/\mu_3, \tag{A.4.e}$$

$$A_{33} = \eta_3(s_{41}\mu_3 + s_{42}/\mu_3 - s_{46}) + s_{45} - s_{44}/\mu_3, \tag{A.4.f}$$

where $\eta_\alpha = -l_3(\mu_a)/l_2(\mu_a)(\alpha = 1,2),\ \eta_3 = -l_3(\mu_3)/l_4(\mu_3).$

In deriving A.2 the standard relationship between roots and coefficients has been used. These algebraic results provide, basically, all that is needed to specialize various solutions.

To gain more insight, orthotropic materials are considered below. The principal axes of each material are considered to be parallel to the *x* and *y* axes, since other orientations may be treated by in-plane rotations and associated tensor rules. Given an orthotropic solid, since s_{16}=s_{26}= 0, only four elastic constants, s_{11}, s_{22}, s_{12}, and s_{66} enter the plane problem formulation. Following the notation introduced earlier (Suo 1990), two non-dimensional parameters are defined as

$$\lambda = s_{11}/s_{22},\ \rho = \frac{1}{2}(2s_{12} + s_{66})(s_{11}s_{22})^{-\frac{1}{2}} \tag{A.5}$$

the characteristic equation A.1 is then

$$\lambda\mu^4 + 2\rho\lambda^{\frac{1}{2}}\mu^2 + 1 = 0. \tag{A.6}$$

The roots with positive imaginary parts are

$$\begin{aligned}
&\mu_1 = i\lambda^{-\frac{1}{4}}(n+m) \quad \mu_2 = i\lambda^{-\frac{1}{4}}(n-m) \quad \text{for } 1<\rho<\infty \\
&\mu_1 = \lambda^{-\frac{1}{4}}(in+m) \quad \mu_2 = \lambda^{-\frac{1}{4}}(in-m) \quad \text{for } -1<\rho<1 \\
&\mu_1 = \mu_2 = -\lambda^{-\frac{1}{4}} \quad \text{for } \rho=1 \\
&n = \left[\tfrac{1}{2}(1+\rho)\right]^{\frac{1}{2}} \qquad m = \left|\tfrac{1}{2}(1-\rho)\right|^{\frac{1}{2}}
\end{aligned} \tag{A.7}$$

The matrix B for an orthotropic material, reduced from A.2 is

$$B = \begin{bmatrix} 2n\lambda^{\frac{1}{4}}(s_{11}s_{22})^{\frac{1}{2}} & i((s_{11}s_{22})^{\frac{1}{2}}+s_{12}) \\ -i((s_{11}s_{22})^{\frac{1}{2}}+s_{12}) & 2n\lambda^{-\frac{1}{4}}(s_{11}s_{22})^{\frac{1}{2}} \end{bmatrix} \tag{A.8}$$

It is interesting to note that B is still well-behaved even if ρ=1 (A and L are singular for this case). The matrix H for the two orthotropic materials with aligned principal axes is

$$H = \begin{bmatrix} H_{11} & -i\beta(H_{11}H_{22})^{\frac{1}{2}} \\ i\beta(H_{11}H_{22})^{\frac{1}{2}} & H_{22} \end{bmatrix} \tag{A.9}$$

where

$$H_{11} = \left\lfloor 2n\lambda^{\frac{1}{4}}(s_{11}s_{22})^{\frac{1}{2}} \right\rfloor_1 + \left\lfloor 2n\lambda^{\frac{1}{4}}(s_{11}s_{22})^{\frac{1}{2}} \right\rfloor_2, \tag{A.10.a}$$

$$H_{22} = \left\lfloor 2n\lambda^{-\frac{1}{4}}(s_{11}s_{22})^{\frac{1}{2}} \right\rfloor_1 + \left\lfloor 2n\lambda^{-\frac{1}{4}}(s_{11}s_{22})^{\frac{1}{2}} \right\rfloor_2, \tag{A.10.b}$$

$$(H_{11}H_{22})^{\frac{1}{2}}\beta = \left\lfloor (s_{11}s_{22})^{\frac{1}{2}} + s_{12} \right\rfloor_2 - \left\lfloor (s_{11}s_{22})^{\frac{1}{2}} + s_{12} \right\rfloor_1, \tag{A.10.c}$$

Here β is a generalization of one of the Dundurs (1969) parameters. The non-oscillatory fields can be obtained by the corresponding results if H is real, or $\beta = 0$. The case $\beta \neq 0$ will be focused below.

The oscillatory index ε, solved from the eigenvalue problem is

$$\varepsilon = (2\pi)^{-1} \ln((1-\beta)/(1+\beta)). \tag{A.11}$$

With the complex stress intensity factor K, the traction in the interface is given by

$$(H_{22}/H_{11})^{\frac{1}{2}}\sigma_{22}+i\sigma_{12}=(2\pi r)^{-\frac{1}{2}}Kr^{i\varepsilon} \tag{A.12}$$

then

$$\begin{aligned}
&K_I+iK_{II}\\
&=\left[\sqrt{\frac{H_{22}}{H_{11}}}\sigma_{22}+i\tau_{12}\right]\left[\cos(\varepsilon\ln r)-i\sin(\varepsilon\ln r)\right]\sqrt{2\pi r}\\
&=\left[\sqrt{\frac{H_{22}}{H_{11}}}\sigma_{22}\cos(\varepsilon\ln r)+\tau_{12}\sin(\varepsilon\ln r)\right]\sqrt{2\pi r}+i\left[\tau_{12}\cos(\varepsilon\ln r)-\sqrt{\frac{H_{22}}{H_{11}}}\sigma_{22}\sin(\varepsilon\ln r)\right]\sqrt{2\pi r}
\end{aligned} \tag{A.13}$$

The energy release rate is thereby

$$G=H_{11}\left|K\right|^2/(4\cosh^2\pi\varepsilon) \tag{A.14}$$

and the phase angle for mode-mixity is

$$\psi=\tan^{-1}\left(\frac{K_{II}}{K_I}\right) \tag{A.15}$$

The stress intensity factors for this case, however defined, may not reduce to the classical definition as the bimaterial degenerates to have $\varepsilon = 0$, because $H22/H11 \neq 1$ if $\lambda \neq 1$. For the case $\varepsilon = 0$ one may rescale $Re(K)$ by $(H22/H11)^{1/2}$ to recover the classical stress intensity factor.

APPENDIX B
EXPERIMENTAL RESULTS AT ROOM TEMPERATURE

Table B.1 Experimental data from sandwich composites with 0.25 inch core

	Front a	Back a	**Avg a**	Distance r	**Work**	Pc	dc	**Gc**
1	0.512	0.383	**0.4475**	2	**0.961**	5.615	0.312	**2.166989**
	1.044	1.062	**1.053**	2.4475	**3.316**	6.578	0.618	**3.177697**
	1.03	1.154	**1.092**	3.5005	**3.919**	6.16	1.351	**3.621421**
	0.942	1	**0.971**	4.5925	**3.397**	4.92	2.242	**3.530227**
2	0.378	0.391	**0.3845**	2	**0.735**	5.8	0.32	**1.892647**
	0.918	0.856	**0.887**	2.3845	**2.453**	5.65	0.495	**2.73812**
	1.286	1.258	**1.272**	3.2715	**4.954**	5.858	1.216	**3.856093**
	0.98	1.119	**1.0495**	4.5435	**3.711**	4.918	2.085	**3.50096**
3	0.53	0.541	**0.5355**	2	**1.206**	5.393	0.337	**2.252101**
	1.22	1.174	**1.197**	2.5355	**3.646**	6.988	0.769	**3.045948**
	1.072	1.032	**1.052**	3.7325	**3.45**	5.975	1.602	**3.279468**
	1.678	1.753	**1.7155**	4.7845	**4.116**	4.582	2.369	**2.3993**
4	0.883	0.74	**0.8115**	2	**1.716**	6.9	0.412	**2.101991**
	1.009	1.069	**1.039**	2.8115	**3.677**	6.816	1.033	**3.517873**
	E	E		3.8505		6.01	1.782	**E**
5	0.598	0.505	**0.5515**	2	**1.014**	6.126	0.353	**1.847861**
	1.056	1.142	**1.099**	2.5515	**3.501**	5.712	0.623	**3.201631**
	1.159	1.198	**1.1785**	3.6505	**3.781**	5.433	1.55	**3.224438**
	0.816	0.865	**0.8405**	4.829	**2.869**	4.099	2.425	**3.430597**

*E: The point that could not get crack propagation due to sudden jump of crack

Table B.2 Experimental data from sandwich composites with 0.5 inch core

	Front a	Back a	**Avg a**	Distance r	**Work**	Pc	dc	**Gc**
1	0.314	0.23	**0.272**	2	**0.435**	6.425	0.314	**1.645334**
	1.004	0.874	**0.939**	2.272	**1.517**	4.836	0.354	**1.662087**
	1	1.19	**1.095**	3.211	**1.994**	4.877	0.866	**1.873461**
	1.01	0.92	**0.965**	4.306	**2.12**	4.03	1.53	**2.260176**
2	0.391	0.357	**0.374**	2	**0.603**	5.54	0.291	**1.662164**
	1.336	1.116	**1.226**	2.374	**2.171**	4.71	0.396	**1.825566**
	1.697	2.047	**1.872**	3.6	**4.613**	5.437	1.152	**2.540422**
3	0.605	0.641	**0.623**	2	**0.688**	5.275	0.289	**1.162457**
	1.013	2.307	**1.66**	2.623	**3.348**	4.06	0.593	**2.123018**
	1.806		**0.903**	4.283				**E**
4	0.459	0.587	**0.523**	2	**0.68**	6.617	0.374	**1.306725**
	1.118	1.036	**1.077**	2.523	**1.849**	6.48	0.632	**1.725433**
	1.019	1.211	**1.115**	3.6	**3.164**	3.857	0.953	**2.851928**
	1.021	0.885	**0.953**	4.715	**2.717**	4.81	2.279	**2.865323**
5	0.379	0.519	**0.449**	2	**0.674**	5.048	0.309	**1.56366**
	2.493	2.549	**2.521**	2.449	**7.029**	5.494	0.663	**2.904353**
	0.934	0.655	**0.7945**	4.97	**2.038**	3.259	2.131	**2.672016**

Table B.3 Experimental data from sandwich composites with 1.0 inch core

	Front a	Back a	**Avg a**	Distance r	**Work**	Pc	dc	**Gc**
1	1.12	0.286	**0.703**	2	**0.771**	4.254	0.259	**1.128321**
	1.566	2.107	**1.8365**	2.703	**1.269**	4.3	0.58	**0.710893**
	1.163	1.015	**1.089**	4.5395	**0.708**	1.6	1.055	**0.668866**
2	0.553	0.503	**0.528**	2	**0.943**	7.379	0.298	**1.77181**
	0.931	1.08	**1.0055**	2.528	**1.74**	6.7	0.45	**1.716748**
	1.221	1.26	**1.2405**	3.5335	**2.514**	5.465	1.02	**2.010518**
	0.915	0.724	**0.8195**	4.774	**1.97**	3.94	0.82	**2.384826**
3	0.624	0.735	**0.6795**	2	**1.539**	8.01	0.327	**2.283166**
	1.253	1.597	**1.425**	2.6795	**3.947**	7.8	0.616	**2.792162**
	1.274	1.262	**1.268**	4.1045	**2.574**	4.73	1.32	**2.046339**
4	0.968	1.041	**1.0045**	2	**1.258**	7.29	0.299	**1.249865**
	0.904	0.71	**0.807**	3.0045	**0.913**	3.77	0.48	**1.129092**
	1.61	1.241	**1.4255**	3.8115	**2.052**	4.92	1.067	**1.436622**

APPENDIX C
EXPERIMENTAL RESULTS AT CRYOGENIC TEMPERATURES

Table C.1 Experimental data from sandwich composites with 0.25 inch core

	Front a	Back a	**Avg a**	Distance r	**Work**	Pc	dc	**Gc**
1	0.551	0.623	**0.587**	2	**0.789**	4.181	0.233	**1.344123**
	1.067	1.203	**1.135**	2.587	**1.992**	4.796	0.492	**1.755066**
	1.274	0.912	**1.093**	3.722	**2.484**	4.38	1.156	**2.272644**
2	0.347	0.389	**0.368**	2	**0.699**	5.93	0.283	**1.899457**
	0.863	0.907	**0.885**	2.368	**1.144**	4.51	0.586	**1.292655**
	1.482	1.59	**1.536**	3.253	**3.251**	5.23	1.089	**2.116536**
3	0.6	0.5	**0.55**	2	**0.932**	7.4	0.345	**1.694545**
	1.147	1.027	**1.087**	2.55	**1.85**	4.81	0.428	**1.701932**
	1.59	1.386	**1.488**	3.637	**2.84**	4.364	1.059	**1.908602**
4	0.545	0.417	**0.481**	2	**0.481**	6.857	0.302	**1**
	1	1.328	**1.164**	2.481	**1.279**	4.154	0.385	**1.098797**
	1.716	1.616	**1.666**	3.645	**2.786**	3.43	0.893	**1.672269**
5	0.494	0.382	**0.438**	2	**0.7**	5.18	0.246	**1.598174**
	1.009	1.15	**1.0795**	2.438	**1.244**	4.88	0.385	**1.152385**
	1.43	1.304	**1.367**	3.5175	**2.611**	3.74	0.963	**1.910022**

Table C.2 Experimental data from sandwich composites with 0.5 inch core

	Front a	Back a	**Avg a**	Distance r	**Work**	Pc	dc	**Gc**
1	0.783	0.624	**0.7035**	2	**0.415**	4.42	0.236	**0.589908**
	1.536	1.81	**1.673**	2.7035	**1.651**	3.52	0.384	**0.98685**
	0.952	0.7	**0.826**	4.3765	**1.17**	2.6	1	**1.416465**
2	0.43	0.394	**0.412**	2	**0.645**	6.13	0.372	**1.565534**
	1.378	1.67	**1.524**	2.412	**1.863**	4.99	0.463	**1.222441**
	1.38	1.015	**1.1975**	3.936	**1.661**	2.82	1.045	**1.387056**
3	0.642	0.557	**0.5995**	2	**0.654**	5.8	0.26	**1.090909**
	1.468	1.766	**1.617**	2.5995	**1.182**	3.63	0.319	**0.730983**
	1.025	1.08	**1.0525**	4.2165	**1.314**	3.96	1.273	**1.248456**
4	0.515	0.435	**0.475**	2	**0.396**	4.488	0.215	**0.833684**
	2.015	2.164	**2.0895**	2.475	**1.57**	3.157	0.278	**0.751376**
	0.762	0.867	**0.8145**	4.5645	**1.676**	3.02	1.82	**2.057704**
5	0.46	0.46	**0.46**	2	**0.205**	5.18	0.184	**0.445652**
	1.763	1.636	**1.6995**	2.46	**1.394**	4.35	0.238	**0.820241**
	1.154	0.937	**1.0455**	4.1595	**1.358**	3.27	1.025	**1.2989**

Table C.3 Experimental data from sandwich composites with 1.0 inch core

	Front a	Back a	**Avg a**	Distance r	**Work**	Pc	dc	**Gc**
1	1.02	0.82	**0.92**	2	**0.74**	5.26	0.194	**0.804348**
	1.762	1.542	**1.652**	2.92	**1.325**	3.34	0.366	**0.802058**
			1.928	4.572	**1.6**	3.47	1.107	**0.829876**
2	0.771	0.726	**0.7485**	2	**0.561**	5.25	0.185	**0.749499**
	2.46	2.43	**2.445**	2.7485	**1.386**	4.86	0.353	**0.566871**
	1.546	1.41	**1.478**	5.1935	**1.85**	1.096	2.99	**1.251691**
3	0.513	0.352	**0.4325**	2	**0.407**	5.91	0.2	**0.94104**
	1.683	1.872	**1.7775**	2.4325	**1.565**	4.1	0.208	**0.88045**
	1.143	1.029	**1.086**	4.21	**0.83**	3.32	0.927	**0.764273**
4	0.552	0.738	**0.645**	2	**0.583**	4.61	0.182	**0.903876**
	0.83	1.375	**1.1025**	2.645	**1.031**	3.68	0.353	**0.935147**
	1.58	1.343	**1.4615**	3.7475	**1.816**	3.35	0.794	**1.242559**

APPENDIX D
MATERIAL INFORMATION OF SANDWICH COMPOSITES AND CURE CYCLE

Honeycomb Core
Designation: ECA, 1/8 inch cell, 4.0 pcf (lb/ft^3)
Manufacturer: Euro-Composites

Unidirectional Carbon Fiber Prepreg
Designation: T800HB-12K-40B/3631, Roll Number B1-210-100-8-1
Manufacturer: Toray Composites (America) Inc.

Vacuum Bag Material
Designation: Econolon Nylon Film
Manufacturer: Airtech International

Breather Material
Designation: Airweave® N-10 $10oz/yd^2$
Manufacturer: Airtech International

Non-Porous Teflon
Designation: NA100-3/38 Non-Porous Teflon Coated fiberglass cloth
Distributor: National Aerospace Supply

Adhesive for Room Temperature
Designation: Epoxy 907 Adhesive System
Manufacturer: Miller-Stephenson chemical co., Inc.

Adhesive for Cryogenic Temperature
Designation: PR-1665
Manufacturer: PRC-DeSoto International

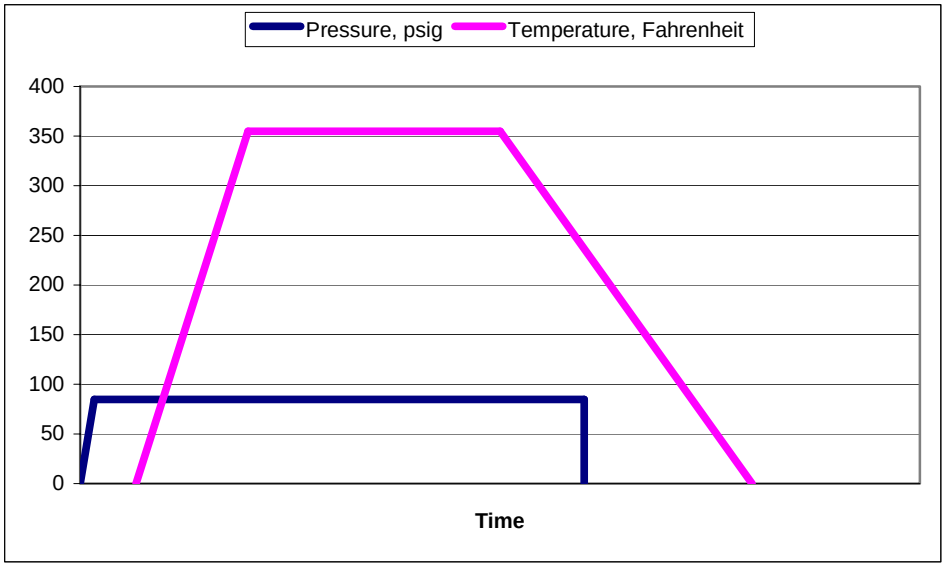

Figure D.1 Toray Composites cure cycle for composite laminates.

1. Apply at least 560 mm (22 inches) Hg vacuum to the bag.

2. Pressurize the autoclave to 6.0 Kgf/cm^2 (85 psig). Vent the vacuum bag to the atmosphere when the pressure reaches 1.4 +0.7/-0.0 kgf/cm^2 (20 +10/-0 psig). Keep the bag vented until the end of the cure. The pressure under the vacuum bag shall be 0 [+0.35/-0.0] kgf/cm^2 (0 [+5/-0] psig) throughout the remainder of the cure cycle.

3. Start the temperature ramp after the autoclave has been fully pressurized.

4. The heat up ramp shall be 1.1 to 2.2 °C/minute (2 to 4 °F/minute). The nominal heat-up rate shall be 1.7 °C/minute (3 °F/minute)

5. Hold for 120 + 60/-0 minutes at 179.5 +/- 5.5°C (355 +/- 10 °F) and 6.0 +1.0/-0.0 kgf/cm^2 (85 +15/-0 psig). The temperature is based on an atmosphere thermocouple. The hold part of the cycle begins when the last thermocouple reaches the minimum cure temperature.

6. Cool down under pressure until the part temperature reaches 60 °C (140 °F) or below The natural pressure drop (1.3 kgf/cm^2 (19 psig) maximum) in the autoclave due to the cool down is allowed. The cool down rate shall be 2.7 °C/minute (5 °F/minute) maximum.

7. When the part temperature reaches below 60°C (140 °F), release the pressure and remove the part.

To prevent from crushing honeycomb core due to pressure, No.3 and No.7 procedures are not applied in this thesis.

APPENDIX E
MATERIAL TESTS RESULTS

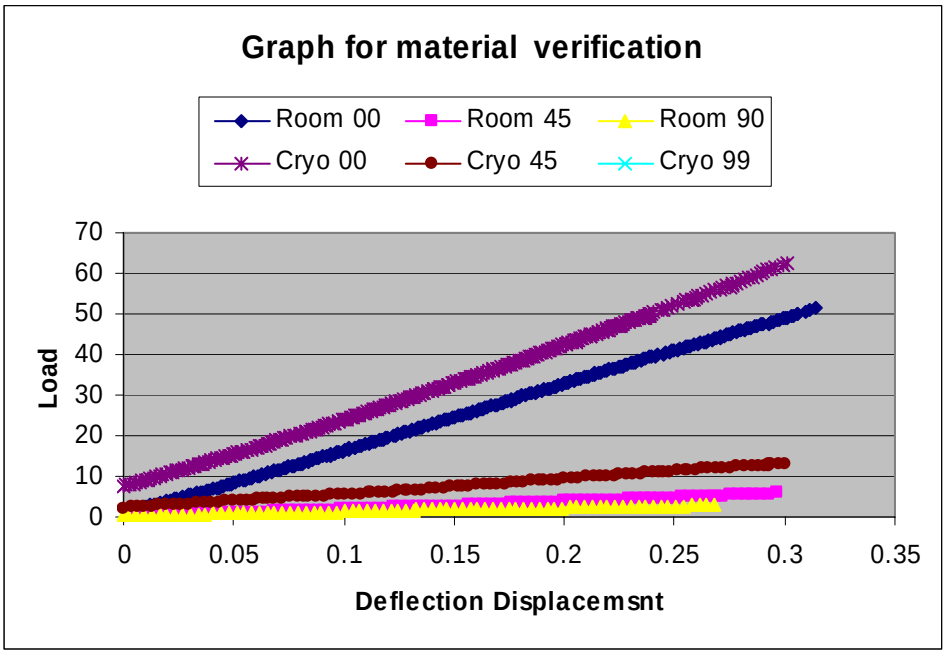

Figure E.1 Load-deflection graph for material property based on temperature and orientation

Table E.1 Experimental results and calculated material properties

	Room	(unit = psi)			
theta	0		45		90
P	20.9135		1.6515		0.9584
delta	0.20035		0.20212		0.20169
	(0.316,51.3)		(0.296,5.75)		((0.306,2.86)
	Ex at 0		**Ex at -45**		**Ex at 90**
	2.09E+07		**2.27E+06**		**1.16E+06**
	E1		**G12**		**E2**
Property	**2.09E+07**		**1.13E+06**		**1.16E+06**

	Cryo	(unit = psi)			
theta	0		45		90
P	23.8391		2.2279		1.4662
delta	0.20039		0.20114		0.20048
	(0.316,57.6)		(0.296,10.9)		(0.306,4.73)
	Ex at 0		**Ex at -45**		**Ex at 90**
	2.34E+07		**4.43E+06**		**1.92E+06**
	E1		**G12**		**E2**
Property	**2.34E+07**		**2.71E+06**		**1.92E+06**

a=1.1 in b=1.0 in h=0.048 in L=5.0 in

LIST OF REFERENCES

1. Ducept, F., Gamby, D. and Davies, P., "A Mixed-Mode Failure Criterion Derived from Tests on Symmetric and Asymmetric Specimens" Composites Science and Technology 1998; 59: 609-619

2. Grau, D., "Relating Interfacial Fracture Toughness to Core Thickness in Honeycomb-Core Sandwich Composites" Master's Degree Thesis, Department of Mechanical and Aerospace Engineering, University of Florida, Gainesville, 2003

3. Schutz, J.B., "Properties of Composite Materials for Cryogenic Applications" Cryogenics 1998; 38(1): 3-12

4. Gates, T.S., Whitley, R.W., Grenoble, R.W. and Bandorawalla, G.T., "Thermal/Mechanical Durability of Polymer-Matrix Composites in Cryogenic Environments" AIAA Journal 2003

5. Bitzer, T., *Honeycomb Technology*, Chapman and Hill, London, 1997

6. Ural, A., Zehnder, A.T. and Ingraffea, A.R., "Fracture Mechanics Approach to Facesheet Delamination in Honeycomb: Measurement of Energy Release Rate of the Adhesive Bond" Engineering Fracture Mechanics 2002; 70: 93-103

7. Suo, Z., "Singularities, Interfaces and Cracks in Dissimilar Anisotropic Media" Proceedings of the Royal Society of London. Series A, Mathematical and Physical Science 1990; 427: 331-358

8. Gibson, R.F., *Principles of Composite Material Mechanics*, McGraw-Hill, New York, 1994

9. Anderson, T.L., *Fracture Mechanics* (2nd Edition) CRC Press LLC, Boca Raton, 1995

10. Charalambides, P.G., Lund, J., Evans, A.G. and McMeeking, R.M., "A Test Specimen for Determining the Fracture Resistance of Bimaterial Interfaces" Journal of Applied Mechanics 1989; 56: 77-82

11. de Morais, A.B., "Double Cantilever Beam Testing of Multidirectional Laminates" Composites Part A: Applied Science and Manufacturing 2003; 34: 1135-1142

12. Hutchinson, J.W. and Suo, Z., "Mixed Mode Cracking in Layered Materials." Advances in Applied Mechanics 1992; 29: 64-163

13. Avery III, J.A. and Sankar, B.V., "Compressive Failure of Sandwich Beams with Debonded Face-Sheets" Journal of Composite Materials 1999; 34: 1176-1199

14. Sun, C.T. and Qian, W. "A Frictional Interfacial Crack under Combined Shear and Compression" Composites Science and Technology 1998; 58: 1753-1761

BIOGRAPHICAL SKETCH

Won-Jong Noh was born in Seoul, Korea, on April 3, 1975 and raised with his generous parents and two adorable sisters. They have supported him physically and mentally throughout his whole life. He has lived his life in a friendly environment surrounded by great people such as his relatives and friends.

He attended schools in Seoul throughout his pre-college career, and then entered the Department of Aerospace and Mechanical Engineering at Hankuk Aviation University in 1994. After taking engineering classes for four years, he established good relationships with his professors and classmates, and also took ROTC training courses during his junior and senior years. After graduating with a Bachelor of Science degree, he served the Republic of Korea Air Force as an engineering officer for three years. In 2002, he wished to pursue deeper study in his major, so he joined Dr. Bhavani V. Sankar's lab, the Center for Advanced Composites at the University of Florida, to study sandwich structures and composites and has studied to get a Master of Science degree.

As the time comes to face the next step of his life, he hopes that it will be filled with great success and plenty of happiness. He will endeavor to do his best to succeed in this new phase of his life.